AD-A052 578 PHYSICS INTERNATIONAL CO SAN LEANDRO CALIF F/G 20/7
OWL II DIODE STUDY.(U)
DEC 77 K CHILDERS, C STALLINGS DNA001-75-C-0110
UNCLASSIFIED PIFR-788 DNA-4432F NL

1 OF 1
AD A
052 578

END
DATE FILMED
5-78
DDC

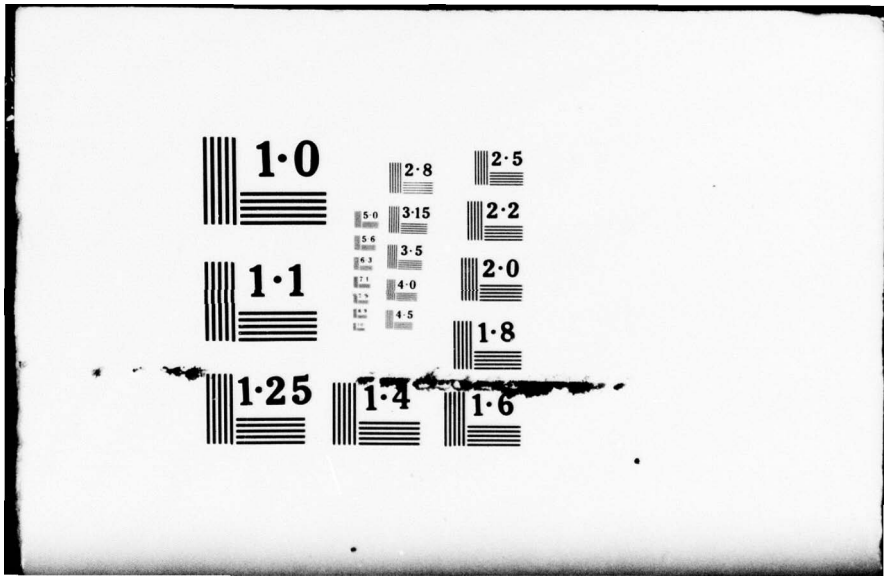
1·0
1·1
1·25
1·4
1·6
1·8
2·0
2·2
2·5
2·8
3·15
3·5
4·0
4·5
5·0
5·6

DNA 4432F

12
B S

OWL II DIODE STUDY

Physics International Company
2700 Merced Street
San Leandro, California 94577

December 1977

Final Report for Period January 1975—April 1975

CONTRACT No. DNA 001-75-C-0110

THIS WORK SPONSORED BY THE DEFENSE NUCLEAR AGENCY
UNDER RDT&E RMSS CODE B342075464 N99QAXAA12112 H2590D.

Prepared for
Director
DEFENSE NUCLEAR AGENCY
Washington, D. C. 20305

Destroy this report when it is no longer needed. Do not return to sender.

(18) DNA, SBIE (19) 4432F, AD-E300 149

UNCLASSIFIED

SECURITY CLASSIFICATION OF THIS PAGE *(When Data Entered)*

REPORT DOCUMENTATION PAGE

READ INSTRUCTIONS BEFORE COMPLETING FORM

1. REPORT NUMBER: DNA 4432F	2. GOVT ACCESSION NO.
3. RECIPIENT'S CATALOG NUMBER: (12) 62p.	
4. TITLE *(and Subtitle)*: (6) OWL II DIODE STUDY.	5. TYPE OF REPORT & PERIOD COVERED: (9) Final Report. [redacted] Jan [redacted]—Apr 75
6. PERFORMING ORG. REPORT NUMBER: (14) PIFR-788	
7. AUTHOR(s): (10) Kendall Childers, Charles Stallings	8. CONTRACT OR GRANT NUMBER(s): (15) DNA 001-75-C-0110
9. PERFORMING ORGANIZATION NAME AND ADDRESS: Physics International Company, 2700 Merced Street, San Leandro, California 94577	10. PROGRAM ELEMENT, PROJECT, TASK AREA & WORK UNIT NUMBERS: (16) NWED Subtask N99QAXA[redacted]12 (17) A121
11. CONTROLLING OFFICE NAME AND ADDRESS: Director, Defense Nuclear Agency, Washington, D.C. 20305	12. REPORT DATE: (11) Dec [redacted]77
	13. NUMBER OF PAGES: 68
14. MONITORING AGENCY NAME & ADDRESS *(if different from Controlling Office)*	15. SECURITY CLASS *(of this report)*: UNCLASSIFIED
	15a. DECLASSIFICATION/DOWNGRADING SCHEDULE

16. DISTRIBUTION STATEMENT *(of this Report)*

Approved for public release; distribution unlimited.

17. DISTRIBUTION STATEMENT *(of the abstract entered in Block 20, if different from Report)*

18. SUPPLEMENTARY NOTES

This work sponsored by the Defense Nuclear Agency under RDT&E RMSS Code B342075464 N99QAXAA12112 H2590D.

19. KEY WORDS *(Continue on reverse side if necessary and identify by block number)*

Electron Beams
Thermal Structural Response Testing

20. ABSTRACT *(Continue on reverse side if necessary and identify by block number)*

An experimental program performed on the OWL II pulsed electron beam accelerator with mean electron energy of 950 keV and electron beam energy of 80 kJ has been accomplished. The reliability of the accelerator was shown to be greater than 90 percent at the 90 percent confidence level. The repeatability of the accelerator can be characterized by ±4 percent MSD (mean square deviation) of beam energy in the diode, ±2 percent MSD of mean electron

DD FORM 1 JAN 73 1473 EDITION OF 1 NOV 65 IS OBSOLETE

UNCLASSIFIED

SECURITY CLASSIFICATION OF THIS PAGE *(When Data Entered)*

+ OR - ± OR - 282760.

20. ABSTRACT (Continued)

energy in the diode, and ±8 percent MSD of average fluence at target location. Electron beams with areas in excess of 400 cm^2, depths of penetration in excess of 0.6 gm/cm^2 and peak doses ranging from 25 to 100 cal/gm were characterized for future thermal structural response testing.

PREFACE

The OWL II Diode Study was conducted by Physics International Company under Defense Nuclear Agency (DNA) Contract DNA-001-75-C-0110. Inclusive dates of research were January 1975 to April 1975.

Program Manager for the program at PI was Mr. Kendall Childers, Program Supervisor was Dr. Charles Stallings, and the Technical Monitor for DNA was Mr. John Farber.

The authors acknowledge the important contributions of Mr. Al York, who designed much of the experimental hardware manufactured in this program and assisted in the laboratory throughout the program, and Drs. Phillip Spence and James Shea, who made many helpful suggestions during the electron beam testing.

CONTENTS

ILLUSTRATIONS

SECTION 1

INTRODUCTION

OWL II is an advanced pulsed electron beam accelerator built for DNA by Physics International Company (Reference 1). The accelerator is capable of delivering electron beams with mean electron energies up to 1.4 MeV and electron beam energies up to 150 kJ (Reference 2). Accelerator reliability has been a problem in the past because of diode insulator breakdowns. In a recently completed internally-funded program, the reliability of OWL II was improved by modifying the diode insulator geometry (Reference 3). The OWL II diode study was initiated to demonstrate accelerator reliability with electron beams suitable for thermal structural response testing.

The objectives of the OWL II Diode Study were to:

(1) Modify the OWL II diode configuration to obtain reliable accelerator performance for nominal electron beam energies of 1 MV.

(2) Demonstrate the statistical reliability of the modified accelerator operating at this voltage level using a 400 cm^2 cathode, with a goal of 90 percent reliability.

(3) Document the results of the testing and define the reliable operating limits of the accelerator.

The goals of this program were met except that the maximum reliable operating limits of the accelerator have not yet been completely defined.

The optimum insulator geometry described in Reference 3 was used for the testing reported here. In addition, the high voltage reliability was further enhanced by improving electrical contact in the cathode current feed. Accelerator reliability was then found to be greater than 90 percent at the 90 percent confidence level, with a 950 keV, 80 kJ electron beam. Moreover, high repeatability of the accelerator was demonstrated, and an entire family of electron beams was characterized for a proposed DNA-funded Lockheed Space and Missile Systems Company (LMSC) thermal-structural response program.

The experimental apparatus and techniques are discussed in Section 2, the experimental results are presented in Section 3, and the conclusions and recommendations are discussed in Section 4.

SECTION 2

EXPERIMENTAL APPARATUS AND TECHNIQUES

2.1 OWL II

A block diagram of OWL II is given in Figure 1. The accelerator is a pulse charged system, consisting of an oil immersed, 1/3 MJ Marx generator and a water-insulated coaxial transmission line pulse transformer, which provides the pulse forming network (Reference 1). The accelerator configuration employed for the testing reported here utilized the 120-nsec pulse line, the 1.8-ohm output impedance transformer, and the recently modified diode insulator geometry.

The electron beam test geometry is shown schematically in Figure 2. The electron beam is generated by a field emission cathode and passes through a transmission anode into the experimental chamber. A magnetic lens* was used to control and transport the electron beam from the cathode emission surface to the target. This produces an electron beam that retains the cross-sectional shape of the cathode but the area of the beam is inversely proportional to the magnetic lens ratio. Fluence uniformity is controlled to first order by dishing the cathode to compensate for the bow of the anode produced by the 1 torr gas pressure in the test chamber.

*For detailed description of a magnetic lens, see References 4 and 5.

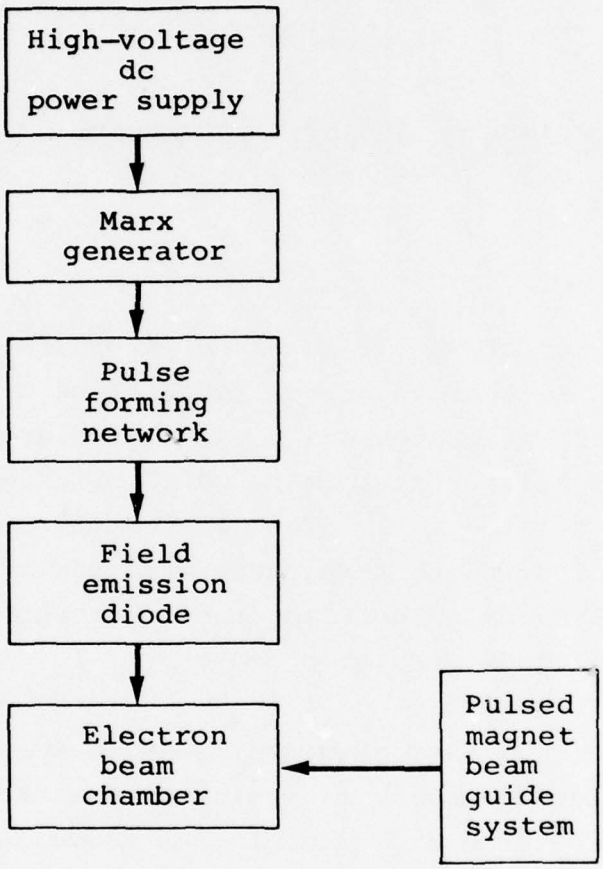

Figure 1 OWL II block diagram.

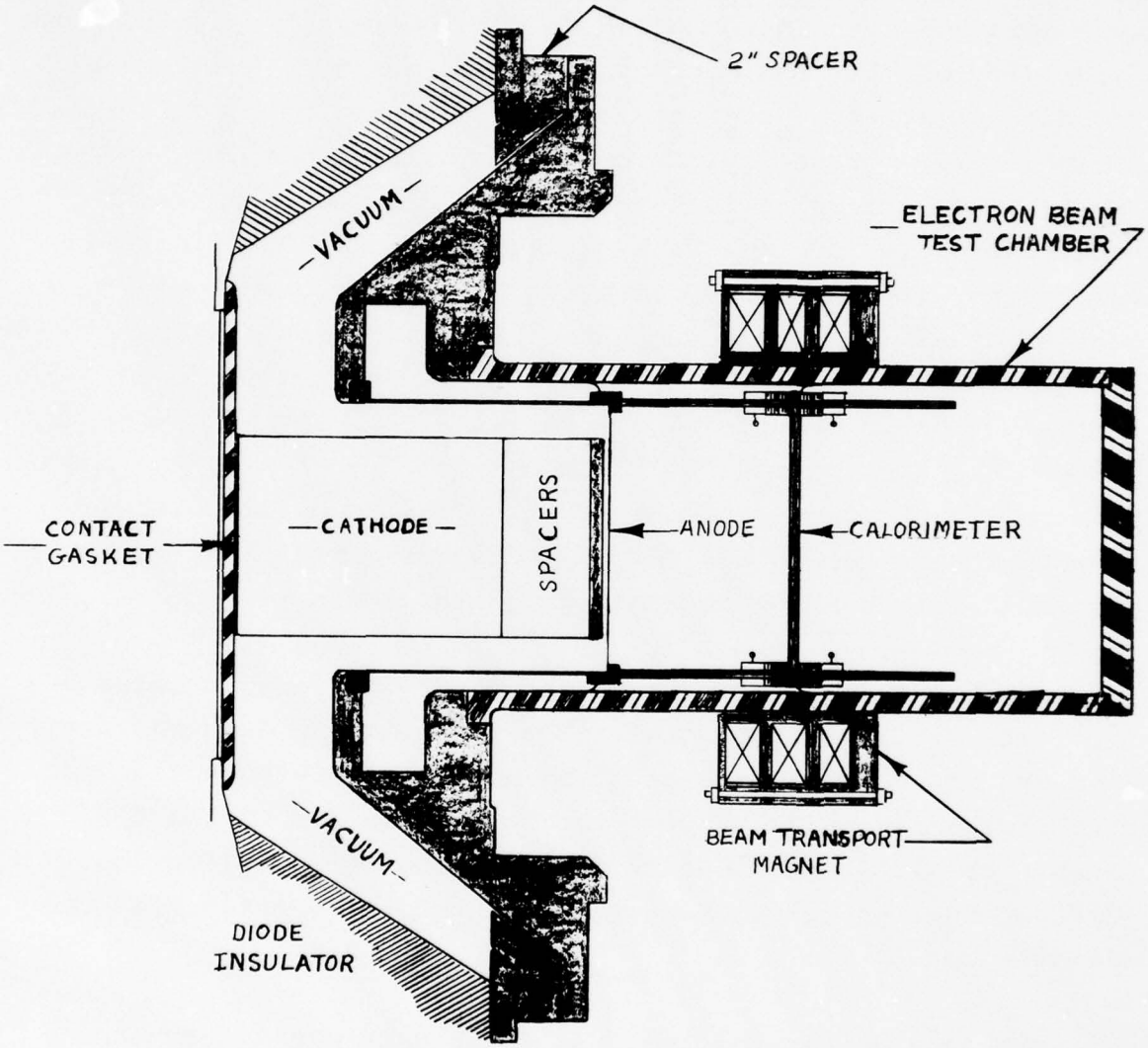

Figure 2 Electron beam test geometry.

2.2 ELECTRON BEAM DIAGNOSTICS

Diagnostics used in characterization of the electron beam were employed both in the diode and at the target location. The diode diagnostics consisted of a voltage monitor, a set of $\dot{B}$ probes, and a set of current monitors. The voltage monitor is a capacitive voltage divider embedded in the diode insulator. The $\dot{B}$ probes are magnetic field sensors that have an output proportional to the time rate of change of the magnetic field associated with the diode current. The diode current monitors consist of Rogowski coil segments that are $\dot{B}$ probes with built-in integrators so that the output is directly proportional to diode current. Four $\dot{B}$ probes and two Rogowski coil segments were on the anode plate located on a diameter just inboard of the inside diameter of the diode insulator. Two full Rogowski coils surrounded the cathode: one was in the anode plate, and the other was in the anode extension near the cathode tip.

The diode diagnostics were recorded with fast oscilloscopes (typically 150 MHz bandwidth). The oscilloscope data was digitized and fed into PI data processing codes (Reference 6). The data processing codes correct the input data for RC and L/R slumps inherent in the monitors, determine the acceleration voltage and then calculate parameters used to characterize the electron beam.

The accelerator voltage, V_{acc}, was determined from the equation:

$$V_{acc} = V_{monitor} - L \frac{dI}{dt}$$

or

$$V_{acc} = V_{monitor} - L \times \left(\text{constant} \times \frac{dB}{dt}\right)$$

where

$V_{monitor}$ is the voltage measured by the voltage monitor after correction for RC slump

L is the diode inductance

I is the diode current

and

constant is the ratio I/B at the location of the $\dot{B}$ probe

The product L x constant was determined by comparing $V_{monitor}$ to the $\dot{B}$ probe when the cathode was shorted to the anode (i.e., $V_{ac} = 0$). Figure 3 shows the results of these calculations for a representative pulse.

The raw oscilloscope data from the current monitors were used separately to determine if, when and where diode insulator breakdown developed in the diode.

The acceleration voltage and diode current waveforms were used directly in the PIEID Monte Carlo code (Reference 7) to calculate electron beam energy deposition profiles for correlation with measurements.

The beam diagnostics at target location consisted of fluence and deposition profile calorimeters. The fluence calorimeter was the closely packed array of total-stopping ATJ graphite blocks, shown in Figure 4. The blocks were mounted on a fiberglass board with aluminum screws which were instrumented with iron-constantan thermocouples. The thermocouple signals were recorded by a scanning digital voltmeter that sampled each probe approximately every 2.2 seconds. The thermal equilibration time was approximately 10 seconds and the thermal decay time was approximately 200 seconds, so the peak thermocouple readings were used to

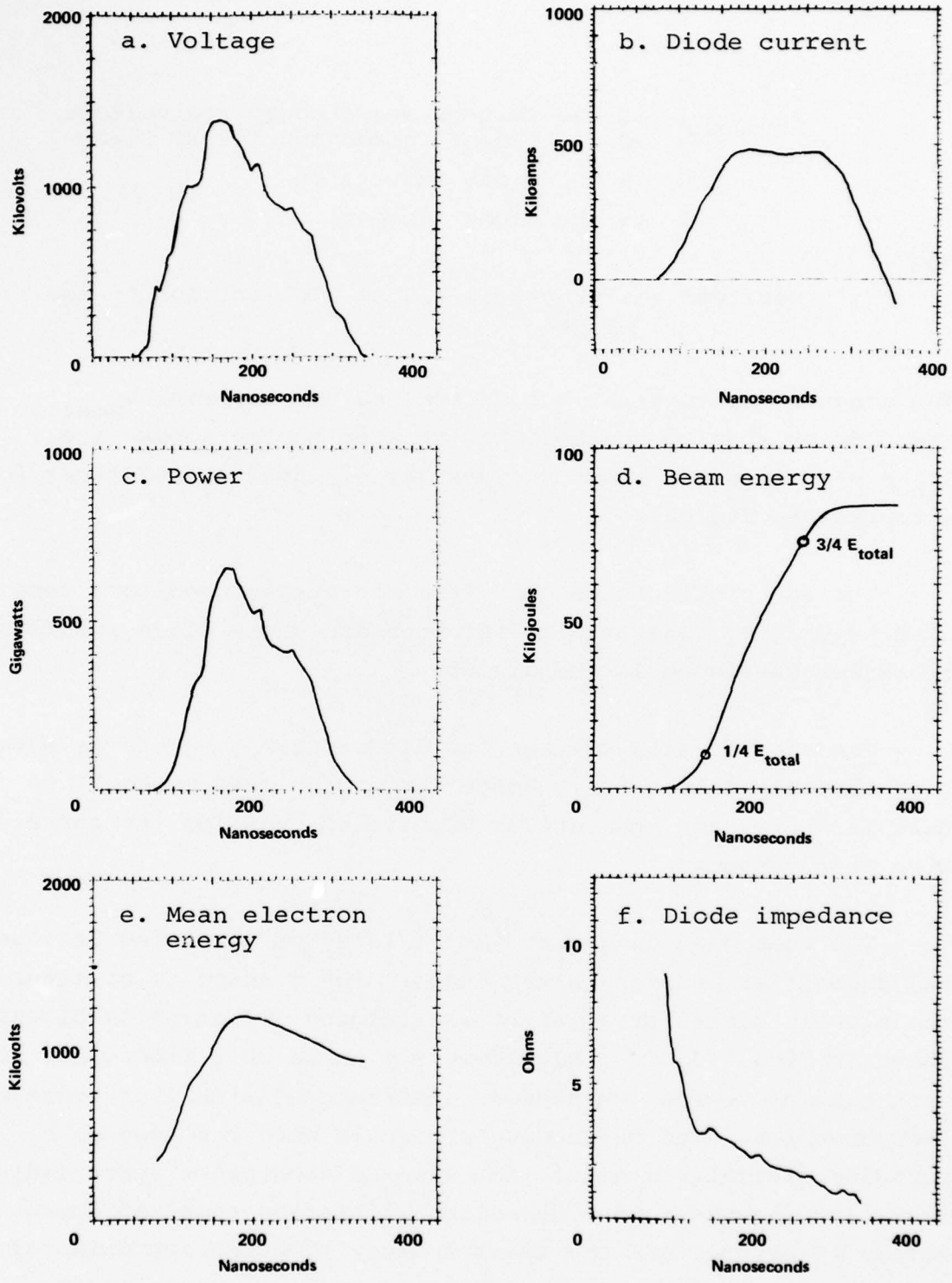

Figure 3 Detailed analysis, OWL II, pulse 2003.

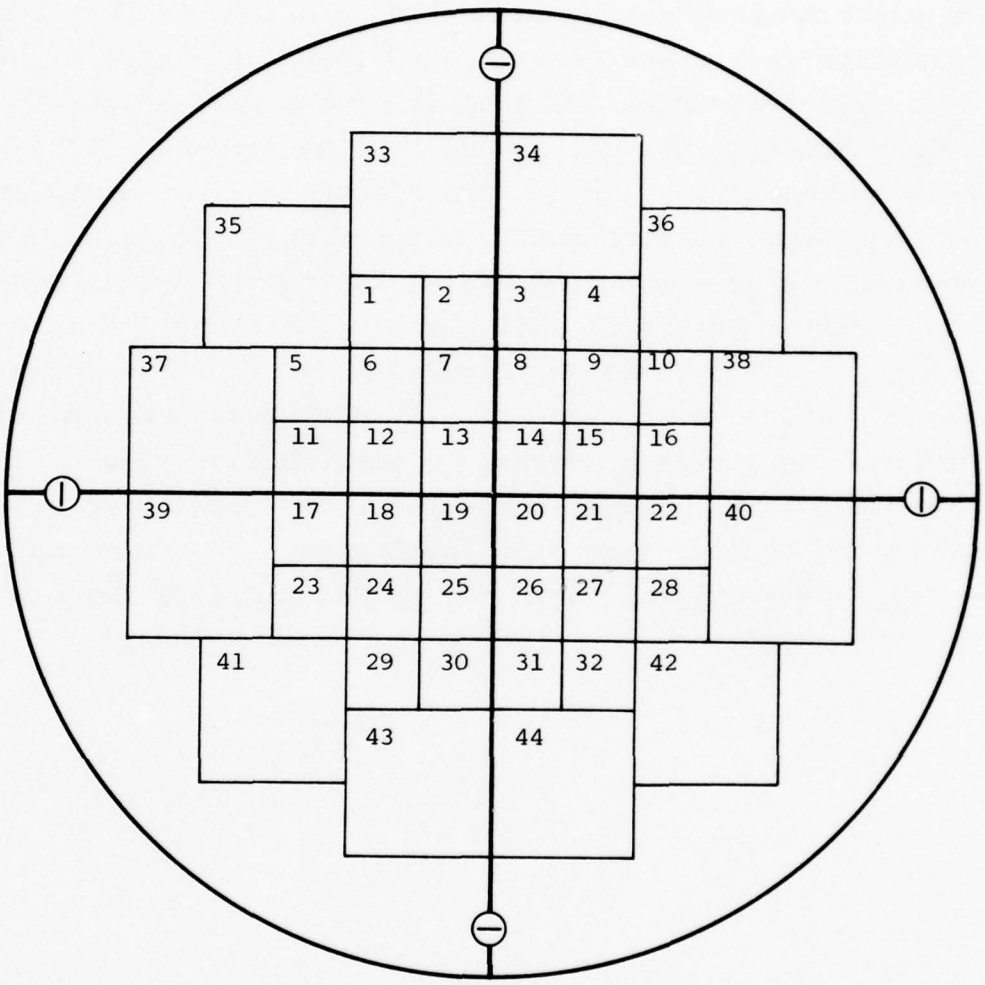

Probes 1 to 32: 1 inch by 1 inch by 0.3 inch

Probes 33 to 44: 2 inches by 2 inches by 0.3 inch

Figure 4 Fluence calorimeter.

determine fluences. Fluences were calculated with a PI mini-computer program, using polynomial fits to handbook enthalpy curves for ATJ graphite and aluminum.

The electron beam energy deposition profile was investigated with a graphite foil stack calorimeter, shown in Figure 5. The foils were 0.02-inch-thick ATJ graphite foils held in position by polyethylene blocks. The foils were instrumented with iron-constantan thermocouples, which were clamped against a copper tab attached to an edge of each foil. The thermocouple signals were read out with the same scanning digital voltmeter system described previously, except that each foil was sampled every 1/2 second, approximately. The thermal equilibration time for the foils was approximately 1 second and the thermal decay time was approximately 20 seconds, so it was necessary to plot thermal response curves and extrapolate to zero-time to determine the deposition profiles. The deposition profiles were calculated with a PI mini-computer program using polynomial fits to the enthalpy curves for ATJ graphite and copper.

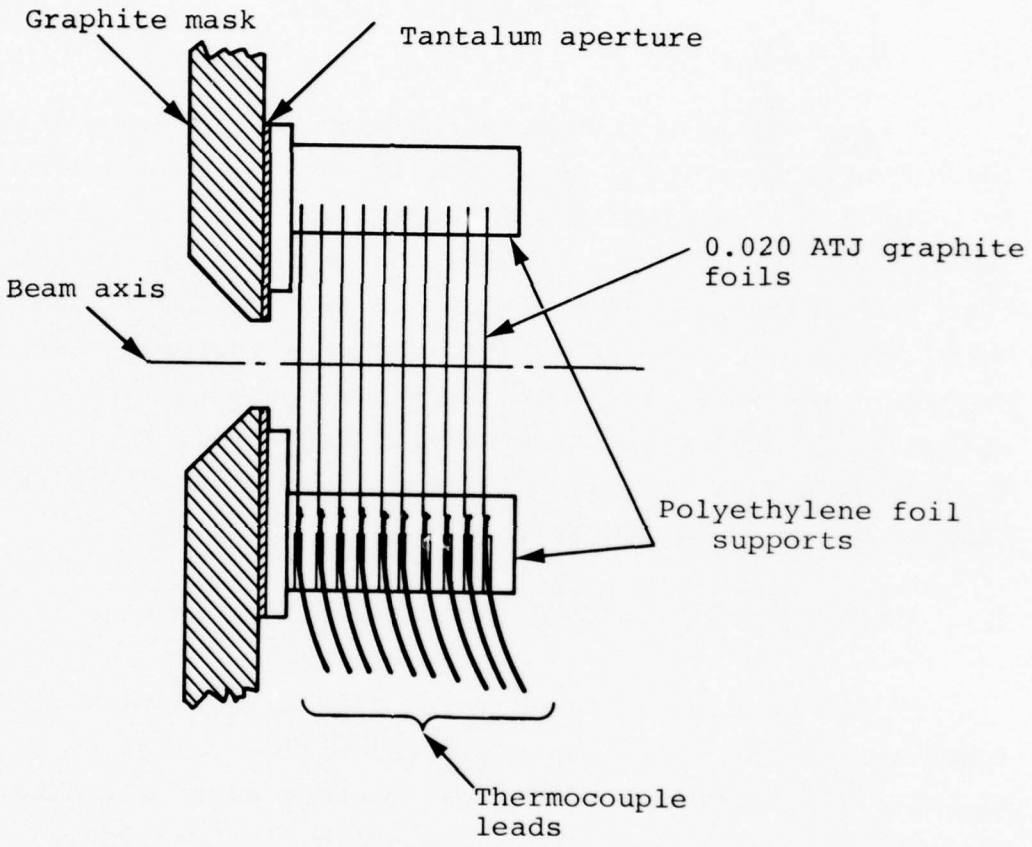

Figure 5 On-axis deposition profile calorimeter.

SECTION 3

EXPERIMENTAL RESULTS

A total of 60 pulses were taken in this program; each of these pulses is briefly described in the pulsing summary table in Appendix A. Approximately two-thirds of these pulses were developmental--improving accelerator reliability, investigating beam uniformity, and determining the best method of producing beams for the proposed DNA/LMSC thermal-structural response program. The final 21 pulses were used to establish accelerator reliability, demonstrate accelerator repeatability, and to characterize electron beams for the proposed DNA/LMSC thermal-structural response program.

3.1 IMPROVEMENT OF ACCELERATOR RELIABILITY

It has been recently observed that illumination of diode insulators with light from the acceleration volume or from arcing at points of imperfect electrical contact adversely affects voltage hold-off capability. Therefore, in preparation for these tests the cathode plate and base of the cathode were machined flat and parallel in an effort to improve electrical contact at the base of the cathode. Furthermore, the cathode spacer rings used to adjust the cathode-anode separation were designed to be placed next to the cathode tip where discontinuities would be hidden from the insulator by the anode extension. These cathode spacer rings were accidently made of aluminum and could not be placed in the pulsed magnetic field (beam guide)

near the cathode tip. Therefore, the initial pulses were attempted with the cathode spacer rings at the cathode base, resulting in poor accelerator reliability. New magnetically transparent cathode spacer rings were made and installed near the cathode tip and reliable accelerator operation was achieved. Eventually the electrical contact at the cathode base degraded and poor accelerator reliability was experienced. The electrical contact at the cathode base was finally assured with a 0.007-inch-thick lead gasket at the cathode base/cathode plate interface. After installing this gasket there was no degradation of accelerator reliability.

3.2 FLUENCE UNIFORMITY

These tests were the first using a transmission anode with the full 400 cm^2 OWL II beam. The initial pulses in this program utilized a 9-inch-diameter cathode tip that was spherically dished by 0.080-inches to investigate the effect of cathode shape on fluence uniformity. This cathode produced a beam that had a thin-intense annulus but good macroscopic fluence uniformity inboard of the annulus. The annulus was sufficiently intense to melt the 0.0005-inch titanium anode, but the central portion of the anode survived and served as a fluence uniformity witness plate. The central portion of the anode showed microscopic fluence irregularities that are characteristic of magnetically controlled electron beams. These microscopic fluence irregularities can be smoothed out by using scattering foils in the electron beam chamber. It was felt that the fluence uniformity was adequate for thermal-structural response testing, so this cathode was used unchanged throughout the testing. The average mean square deviation (MSD) macroscopic-fluence uniformity in this program was ± 7 percent.

3.3 FLUENCE LEVELS

The fluence levels were changed by varying the magnetic lens ratio, the ratio of magnetic field strength at target location to magnetic field strength at the cathode emission surface. To first order, the fluence level should be directly proportional to the lens ratio, L. Several different magnet positions were investigated and it was found that the magnet position could be fixed and the fluence levels for the proposed DNA/LMSC thermal-structural response program could be generated with one set of accelerator parameters by simply changing the position of the target. The lens ratio as a function of distance from the cathode for this geometry is shown in Figure 6.

3.4 OWL II RELIABILITY

The 21 consecutive pulses listed in Table 1 established the reliability of OWL II at design output levels. There were no diode insulator breakdowns in these 21 consecutive pulses. With no failures in 21 "observations," the probability of success is greater than 90 percent at the 90 percent confidence level, based on statistical analysis assuming binomial probability distribution (Reference 8).

3.5 OWL II REPEATABILITY

These data can be used to demonstrate the repeatability of OWL II. The repeatability of the pulser (up to the diode), characterized by the pulse charge, has always been good. For this series the pulse charge was repeatable to ±1 percent MSD (ignoring pulse 2020, for which the pulse charge was intentionally reduced). The repeatability of the accelerator characterized by diode performance has been a problem in the past because of diode insulator breakdowns. In these tests the repeatability

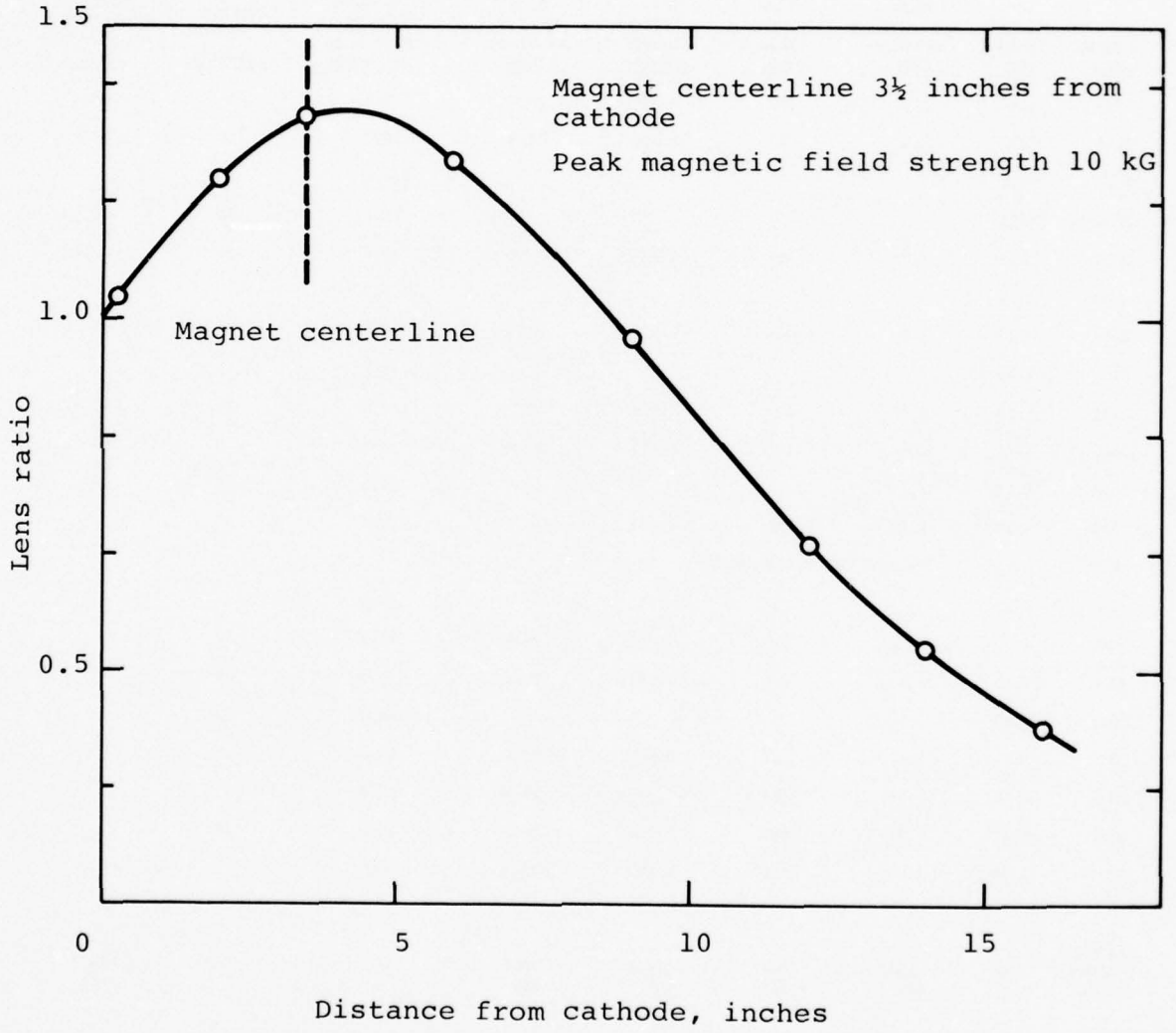

Figure 6 Magnetic lens ratio.

TABLE 1

DATA SUMMARY

Pulse Number	Pulse Charge (MV)	Peak Acceleration Voltage (MV)	Peak Beam Current (kA)	Mean Electron Energy (MeV)	Beam Energy in Diode (kJ)	Calorimeter Position (inches from Cathode)	Average Fluence (cal/cm^2)	Beam Energy Deposited in Calorimeter (kJ)
2003	3.22	1.39	480	0.934	83.0	8.5	41	66.5
2004	3.22	1.28	443	0.898	75.0	10.0	28	59.3
2005	3.13					10.6		
2006	3.13					10.0	30	62.5
2007	3.13	1.39	455	0.934	77.8	9.5	34	63.6
2008	3.13					9.1		
2009	3.13	1.40	459	0.952	77.6	10.0	31	~63.0
2010	3.13					9.1		
2011	3.13	1.41	473	0.946	79.9	8.5	39	66.0
2012	3.13	1.43	465	0.955	81.6	8.5		
2013	3.13					8.5	43	69.3
2014	3.13	1.39	468	0.925	80.6	8.5		
2015	3.13	Bz BANK DID NOT TRIGGER						
2016	3.13					8.5		
2017	3.13	1.36	495	0.910	86.8	12.0	24	
2018	3.13	1.37	466	0.944	79.6	14.0	17	
2019	2.88					14.0	12	
2020	3.13	1.44	447	0.973	76.8	16.0	12	
2021	3.22	1.39	488	0.957	82.5	16.0		
2022	3.13	1.31	460	0.924	76.1	16.0	9	
2023	3.00	1.25	454	0.898	71.3	8.5		
Average Values ± MSD	3.14 ±1%	1.37 ±4%	466 ±3%	0.935 ±2%	78.7 ±4%			64.3 ±5%

NOTE: 1. There were NO diode insulator breakdowns.

2. For pulse 2019, the pulse charge was intentionally reduced and the cathode-anode separation was increased in an attempt to reduce the fluence but retain (the high) electron energy.

of beam parameters in the diode was quite good. Considering the thirteen pulses for which detailed beam characterization analysis was performed, the peak acceleration voltage was repeatable to ±4 percent MSD, the peak diode current was repeatable to ±3 percent MSD, the mean electron energy was repeatable to ±2 percent MSD, and the beam energy in the diode was repeatable to ±4 percent MSD.

The repeatability of the electron beam loading conditions at target location is more difficult to assess because the data were collected at several fluence levels. From the beam characterization analysis below, the beam fluence at a given position is repeatable to about ±8 percent MSD. The electron beam energy deposition profile measurements are insufficient to determine repeatability of the energy deposition profile with confidence.

3.6 BEAM CHARACTERIZATION ANALYSIS

The beam characterization analysis seeks to define the electron beam loading conditions for a data pulse that usually has no beam diagnostics at target location. With magnetically guided beams there is usually a well-defined relationship between the electron beam loading conditions at target location and electron beam parameters in the diode.

First note that the beam transport efficiency, η:

$$\eta = \frac{\text{Beam energy deposited in the calorimeter}}{\text{Beam energy in the diode}}$$

is 0.81 ±2 percent MSD on the pulses for which the active area of the calorimeter intercepts the entire beam (pulses 2003, 2004, 2006, 2007, 2011, and 2013). The fluence level as a function of position from the distance from the cathode can then be calculated (see Figure 7):

$$\phi_c(z) = \frac{0.81 * E_D * L(z)}{A_c}$$

$\phi_c(z)$ is calculated fluence in cal/cm^2 as a function of distance from cathode, z.

0.81 is energy transport efficiency

E_D is diode energy in calories (average value for this series = $18.8 * 10^3$ calories)

L(z) is magnetic lens ratio as a function of distance from cathode, z.

A_c is area of cathode in cm^2 (410 cm^2 for this series)

The measured fluence levels from Table 1 are plotted on Figure 7 for comparison. The correlation is excellent; the measurements agree with the calculated values to ±8 percent MSD.

Measured electron beam energy deposition profiles were compared to values calculated, utilizing acceleration voltage and diode current waveforms to determine the mean angle of incidence of the electron beam. This correlation was attempted

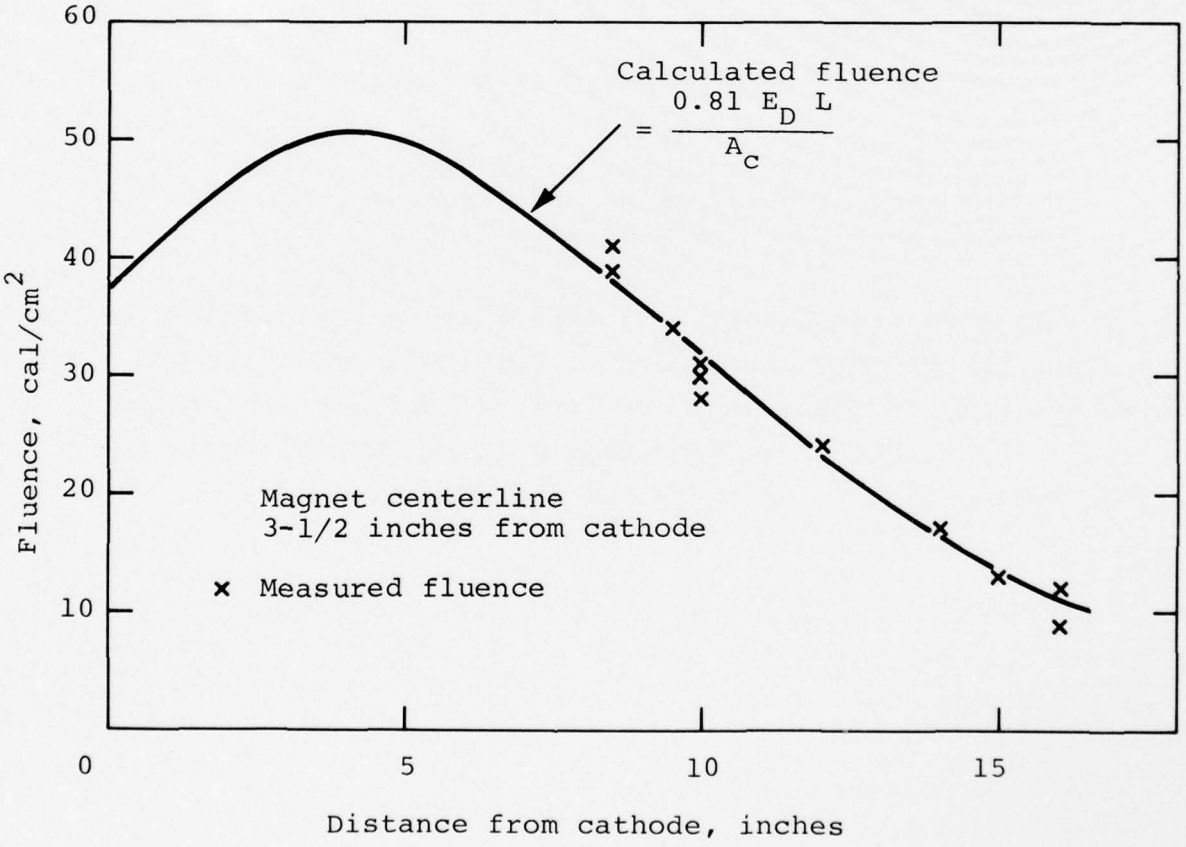

Figure 7 Axial fluence map.

at the fluence levels of interest for the proposed DNA/LMSC thermal-structural response program, i.e., 40 cal/cm^2 and 10 cal/cm^2. Excellent agreement was found between measurements and values calculated with normal incidence for pulses 2012 and 2014 (Figures 8a and 8b), but only qualitative agreement was found for pulses 2021 and 2023 (Figures 9a and 9b); the discrepancy is discussed in Appendix C.

Based upon the results obtained in this study, the electron beam loading conditions for any pulse can be determined for this diode configuration according to the following procedure:

1. The fluence is determined from Figure 7.

2. The electron beam energy deposition profile is calculated, using acceleration voltage and diode current waveforms, assuming that the electrons are normally incident on the target.

This kind of analysis will typically be performed after an electron beam testing sequence, but it is expensive and time consuming. These data were used to develop an on-line method of estimating electron beam loading conditions in the laboratory, which is presented in Appendix D.

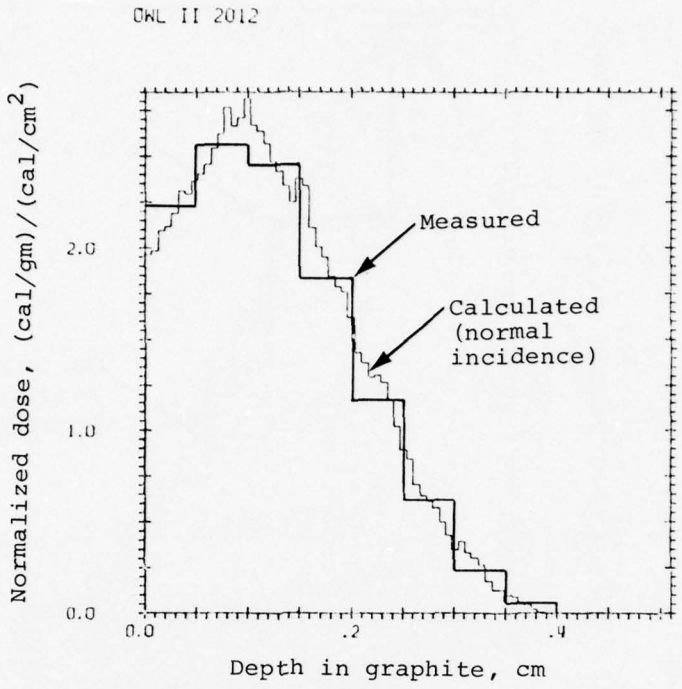

a.

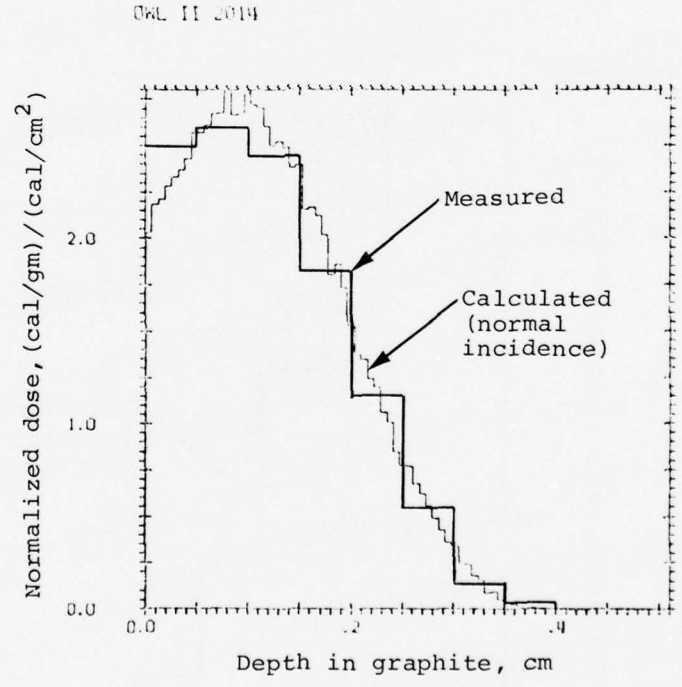

b.

Figure 8 Correlation between measured and calculated electron beam energy deposition profiles.

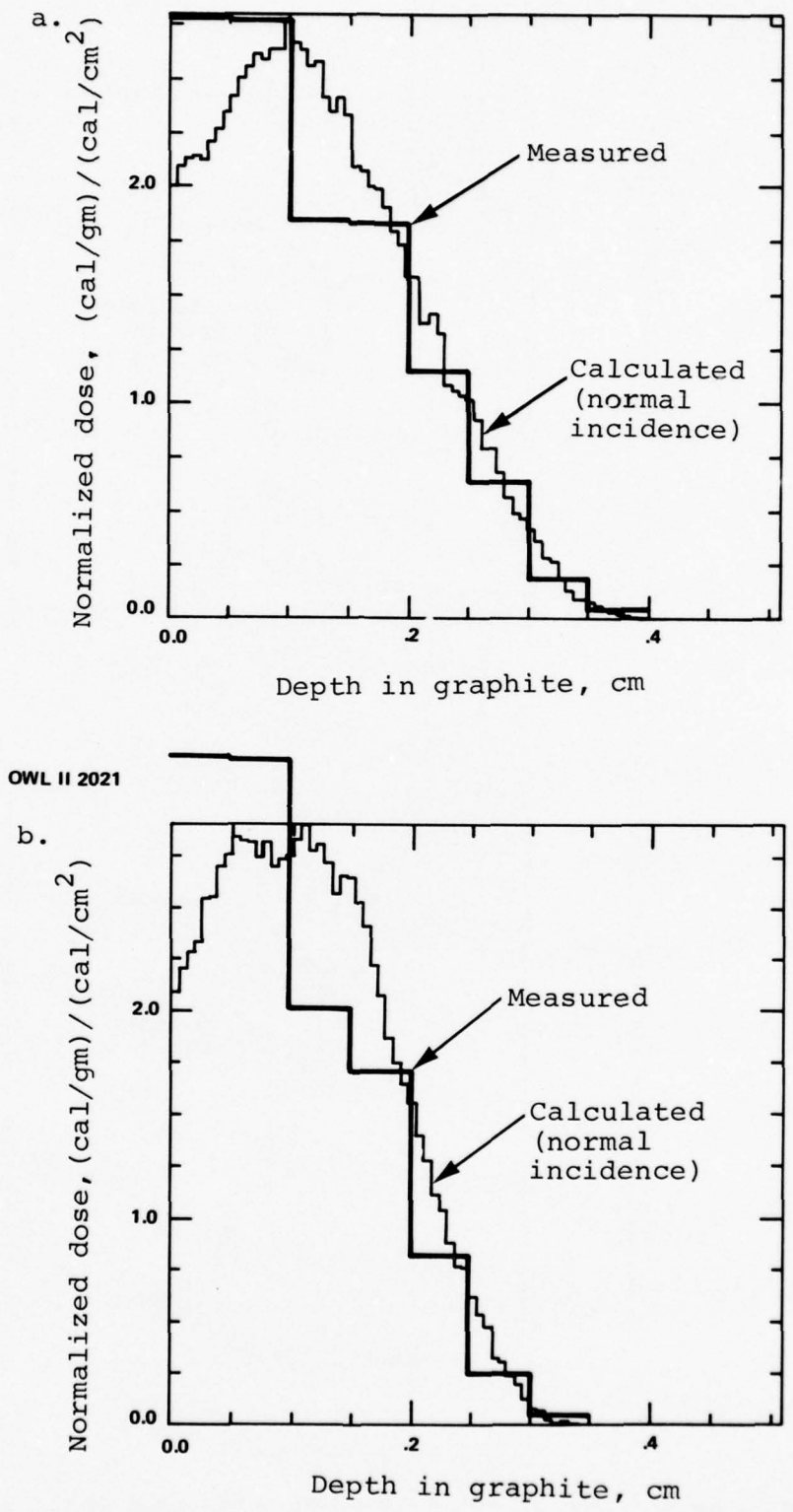

Figure 9 Correlation between measured and calculated electron beam energy deposition profiles.

SECTION 4

CONCLUSIONS AND RECOMMENDATIONS

OWL II has been shown to be a reliable, repeatable accelerator with a 950 keV 80 kJ electron beam. This electron beam is available for thermal-structural response testing with areas in excess of 400 cm^2, depths of penetration greater than 0.6 gm/cm^2, and peak doses ranging from 25 to 100 cal/gm.

The successful completion of this program gives impetus to the further development of high dose OWL II electron beams for material response testing. Reliable operation of the OWL II insulator will allow developmental efforts to concentrate on elimination of early diode impedance collapse problems that have adversely affected accelerator repeatability for high current density beams.

REFERENCES

1. K. Nielsen, G. Frazier, and P. Spence, OWL II Generator Enhancement and Electron Beam Characterization (Private Communication).

2. G. B. Frazier, (Physics International Company, San Leandro, California), The OWL II Pulsed Electron Beam Generator, presented at the 13th Symposium for Electron, Ion, and Photon Technology, Colorado Springs, Colorado, May 22, 1975.

3. P. Spence, OWL II Diode and Insulator Studies, Physics International Internal Memo, Physics International Company, November 1974.

4. C. Stallings, K. Childers and S. Shope, High Dose Test Capability, PIFR-409, Physics International Company, March 1975.

5. K. Childers and J. Shea, Material Response Technology on The Physics International Mylar Line, PIFR-423-2, Physics International Company, November 1974.

6. H. Calvin and N. Bergstrom, Computerized Data Reduction, PIIR-2-75, Physics International Company, March 1975.

7. J. Reaugh and L. Behrmann, Documentation of the Physics International Monte Carlo Electron Transport Computer Code, PIIR-9-71, Physics International Company, January 1971.

8. J. O. Muench, The Cumulative Binomial Distribution Computer, SC-R-64-1348 and TID-4500, Sandia Corporation, Albuquerque, New Mexico, October 1964.

APPENDIX A

PULSING SUMMARY

This Appendix describes briefly every pulse taken in this program. The supporting data, calorimeter fluence maps, and measured electron beam energy deposition profiles, are presented in Appendices B and C.

TABLE A-1

Pulse	Pulse Charge (MV)	Cathode Anode Separation (cm)	Peak Diode Voltage (MV)	Peak Acceleration Voltage (MV)	Peak Diode Current (kA)	Target*	Target Position (Inches from Cathode)	Magnet Position Distance Between Centerline of Magnet and Cathode (Inches)	Average Fluence Over Central 32 sq. in. (cal/cm^2)	Beam Energy Deposited in Calorimeter (kJ)	Comments
1964	1.9	0	0.7	0	680	None					Determine diode inductance
1965	1.8	0	0.7	0	660	None					Determine diode inductance
1966	1.7	0	0.6	0	630	None					Determine diode inductance
						INSTALL ALUMINUM CATHODE SPACERS AT CATHODE TIP					
1967	2.9	2.5	1.7	1.6	260	Fluence Calorimeter	5	4			Diode insulator breakdown
						INSTALL ALUMINUM CATHODE SPACERS AT CATHODE BASE					
1968	2.7	2.5	1.7	1.5	270	Fluence Calorimeter	4½	4			Diode insulator breakdown
1969	3.0	2.0	1.6	1.4	400	Fluence Calorimeter	4½	4	54	59	Good pulse
1970	3.0	1.75	1.5	1.0	290	Fluence Calorimeter	4½	2½	--	--	Diode insulator breakdown
1971	3.2	1.6	1.5	1.0	360	Fluence Calorimeter	4½	½	--	--	Diode insulator breakdown
1972	3.2	1.6	1.6	1.3	480	Fluence Calorimeter	4½	½	--	--	Diode insulator breakdown
						INSTALL GRAPHITE CATHODE SPACERS AT CATHODE TIP					
1973	2.8	1.5	1.4	1.0	630	Fluence Calorimeter	4½	½	23	56	Good pulse
1974	3.1	2.0	1.8	1.7	380	Fluence Calorimeter					Magnet bank did not fire--diode insulator breakdown
1975	3.2	2.0	1.6	1.3	390	Fluence Calorimeter	4½	½	26	57	Asymmetric current feed--excessive shank emission
1976	3.2	2.0	1.5	1.3	400	Fluence Calorimeter	4½	4½	47	62	Good pulse
1977	3.4	2.0	1.6	1.5	370	Fluence Calorimeter	4½	½	25	63	Asymmetric current feed--excessive shank emission
1978	3.6	2.0	---	---	---						Magnet bank did not fire--diode insulator breakdown
1979	3.3	2.0	1.6	1.3	450	Fluence Calorimeter	10½	½	12½	*	Late diode insulator breakdown
1980	3.4	2.0	1.6	1.4	470	Fluence Calorimeter	4½	3½	44	64	Good pulse
1981	3.5	2.0	1.6	1.4	470	Deposition Profile Calorimeter	5-1/16	½			Asymmetric current feed--late diode insulator breakdown
1982	3.3	2.0	1.8	1.5	520	Deposition Profile Calorimeter	5-1/16	½			Asymmetric current feed--late diode insulator breakdown
1983	3.4	2.0	1.6	1.4	470	Deposition Profile Calorimeter	5-1/16	3½			Good pulse
1984	3.3	2.0	---	---	---						Magnet bank did not fire--diode insulator breakdown
1985	3.3	2.0	1.6	1.4	450	Fluence Calorimeter	15	3½	13	*	Good pulse

*Calorimeter did not intercept entire beam.

TABLE A-1 (cont.)

Pulse	Pulse Charge (MV)	Cathode Anode Separation (cm)	Peak Diode Voltage (MV)	Peak Acceleration Voltage (MV)	Peak Diode Current (kA)	Target	Target Position (Inches from Cathode)	Magnet Position Distance Between Centerline of Magnet and Cathode (Inches)	Average Fluence Over Central 32 sq. in. (cal/cm^2)	Beam Energy Deposited in Calorimeter (kJ)	Comments
						INSTALL TOTAL STOPPING GRAPHITE ANODE					
1986	3.2	2.05	1.7	1.5	450	None		3½			Diode insulator breakdown
1987	3.3	1.95	1.7	1.4	450	None		3½			Good pulse
1988	3.4	1.95	2.1	2.0	---			--			Magnet bank did not fire-- diode insulator breakdown
1989	3.3	1.95	1.7	1.3	390	None		½			Diode insulator breakdown
1990	3.2	1.95	1.7	---	420	None		3½			Diode insulator breakdown
1991	3.4	1.85	1.7	1.4	520	None		3½			Good pulse
1992	3.4	1.85	---	---	---	None		--			Magnet bank did not fire-- diode insulator breakdown
1993	3.4	1.85	1.6	1.3	600	None		3½			Diode insulator breakdown
						TIGHTEN CATHODE TO CATHODE PLATE					
1994	3.9	1.55	1.8	1.3	770	None		3½			Diode insulator breakdown
						POLISH CATHODE BASE AND CATHODE PLATE AND IMPROVE ANODE CURRENT RETURN					
1995	3.1	1.85	1.6	1.4	500	None		3½			Good pulse
1996	3.1	1.85	1.5	1.2	630	None		3½			Good pulse
1997	3.2	1.85	1.6	1.3	600	None		3½			Good pulse
1998	3.1	2.05	---	---	---			--			Magnet bank did not fire-- diode insulator breakdown

TABLE A-1 (cont.)

Pulse	Pulse Charge (MV)	Cathode Anode Separation (cm)	Peak Diode Voltage (MV)	Peak Acceleration Voltage (MV)	Peak Diode Current (kA)	Target	Target Position (Inches from Cathode)	Magnet Position Distance Between Centerline of Magnet and Cathode (Inches)	Average Fluence Over Central 32 sq. in. (cal/cm^2)	Beam Energy Deposited in Calorimeter (kJ)	Comments
1999	3.2	1.85									Magnet bank did not fire-- diode insulator breakdown
2000	3.3	1.85	1.7	1.5	500	Fluence Calorimeter		3½	49	68	Good pulse
2001	3.2	1.85	1.7	1.5	470	Fluence Calorimeter		3½			Diode insulator breakdown
2002	3.3	1.85	1.8	1.2	420	Fluence Calorimeter		3½			Diode insulator breakdown
						INSTALL LEAD GASKET AT CATHODE BASE START RELIABILITY RUN					
2003	3.2	1.85	1.7	1.4	470	Fluence Calorimeter		3½	41	67	Good pulse
2004	3.2	1.85	1.6	1.3	430	Fluence Calorimeter		3½	28	59	Good pulse
2005	3.1	1.85	1.6	1.4	470	Deposition Profile Calorimeter					Good pulse
2006	3.1	1.85	1.6	1.4	430	Fluence Calorimeter		3½	30	62	Good pulse
2007	3.1	1.85	1.6	1.4	450	Fluence Calorimeter		3½	34	64	Good pulse
						FIX MAGNET BANK					
2008	3.1	1.85	1.8	1.4	460	Deposition Profile Calorimeter		3½			Good pulse
2009	3.1	1.85	1.7	1.4	450	Fluence Calorimeter		3½			Good pulse
2010	3.1	1.85	1.7	1.4	470	Deposition Profile Calorimeter		3½	31	63	Good pulse
2011	3.1	1.85	1.7	1.4	470	Fluence Calorimeter		3½	39	66	Good pulse
2012	3.1	1.85	1.7	1.4	450	Deposition Profile Calorimeter		3½			Good pulse
2013	3.1	1.85	1.6	1.4	430	Fluence Calorimeter		3½	43	69	Good pulse
2014	3.1	1.85	1.6	1.4	470	Deposition Profile Calorimeter		3½			Accelerator triggered early $B_z \sim 2/3\ B_z$ max Good pulse
2015	3.1	1.85	1.7	1.7	420						Accelerator triggered early $B_z = 0$; NO diode insulator breakdown
2016	3.1	1.85	1.7	1.4	450	Deposition Profile Calorimeter		3½			Good pulse; lost first foil in calorimeter
2017	3.1	1.85	1.7	1.4	470	Fluence Calorimeter		3½	24	*	Good pulse
2018	3.1	1.85	1.7	1.4	450	Fluence Calorimeter		3½	17	*	Good pulse
						DECREASE PULSE CHARGE AND INCREASE CATHODE-ANODE SEPARATION TO DECREASE FLUENCE BUT MAINTAIN VOLTAGE					
2019	2.9	2.05	1.5	1.2	370	Fluence Calorimeter		3½	12	*	Good pulse
						GO BACK TO ORIGINAL PULSE CHARGE AND CATHODE-ANODE SEPARATION					
2020	3.1	1.85	1.7	1.4	450	Fluence Calorimeter		3½	12	*	Good pulse
2021	3.2	1.85	1.7	1.4	470	Deposition Profile Calorimeter		3½			Good pulse
2022	3.1	1.85	1.6	1.3	420	Fluence Calorimeter		3½	9	*	Good pulse
2023	3.0	1.85	1.6	1.2	393	Deposition Profile Calorimeter		3½			Good pulse

APPENDIX B

FLUENCE CALORIMETER DATA

This Appendix presents the individual calorimeter fluence maps taken in this program. The data for pulses with diode insulator breakdowns have been deleted.

On some of the pulses, data was lost from some calorimeter probes. On these pulses the beam energy deposited in the calorimeter was estimated by assuming that the missing probes had the average energy deposited in the other probes (this was done separately for the 1-inch square probes and the 2-inch square probes).

Top

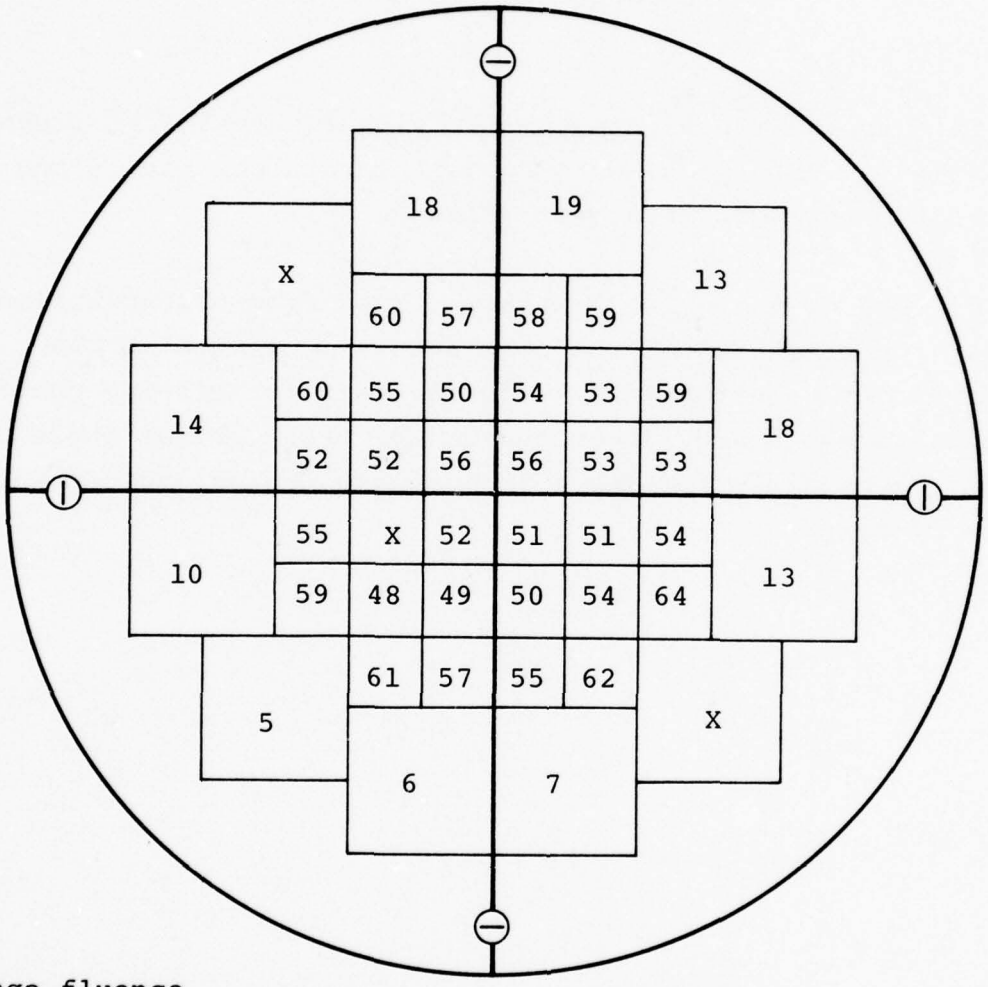

Average fluence
over central 32 square inches = 54 cal/cm^2 ±7% MSD

Energy deposited = 59 kJ

Figure B-1 Fluence map, pulse 1969.

Top

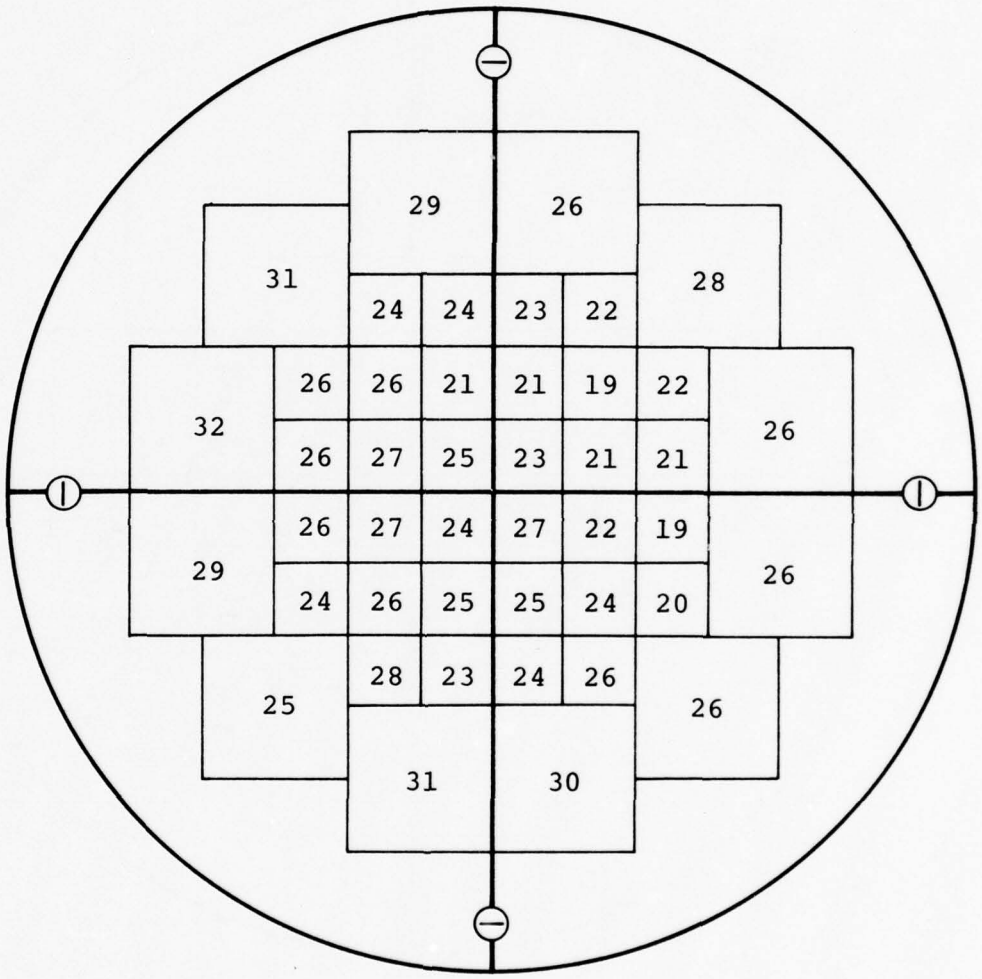

Average fluence
over central 32 square inches = 23 cal/cm^2 ±10% MSD

Energy deposited = 56 kJ

Figure B-2 Fluence map, pulse 1973.

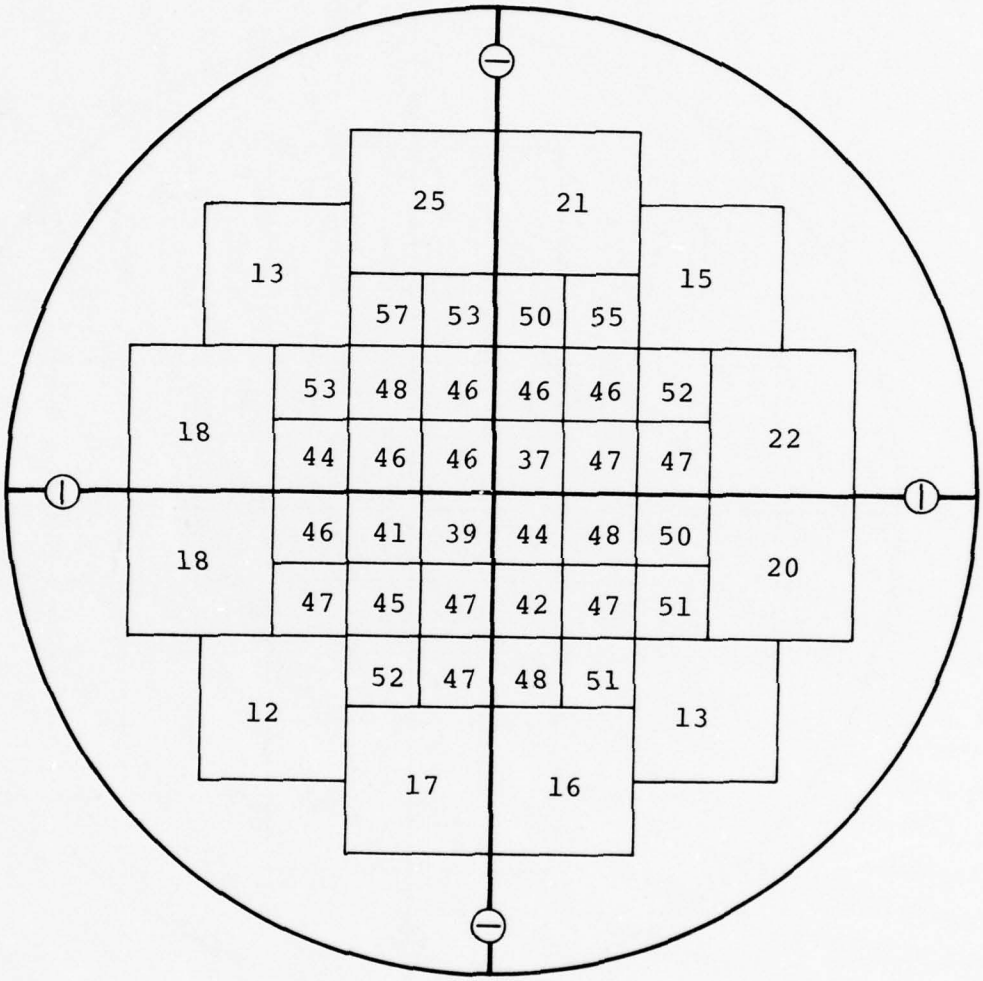

Average fluence
over central 32 square inches = 47 cal/cm^2 ±9% MSD
Energy deposited = 62 kJ

Figure B-3 Fluence map, pulse 1976.

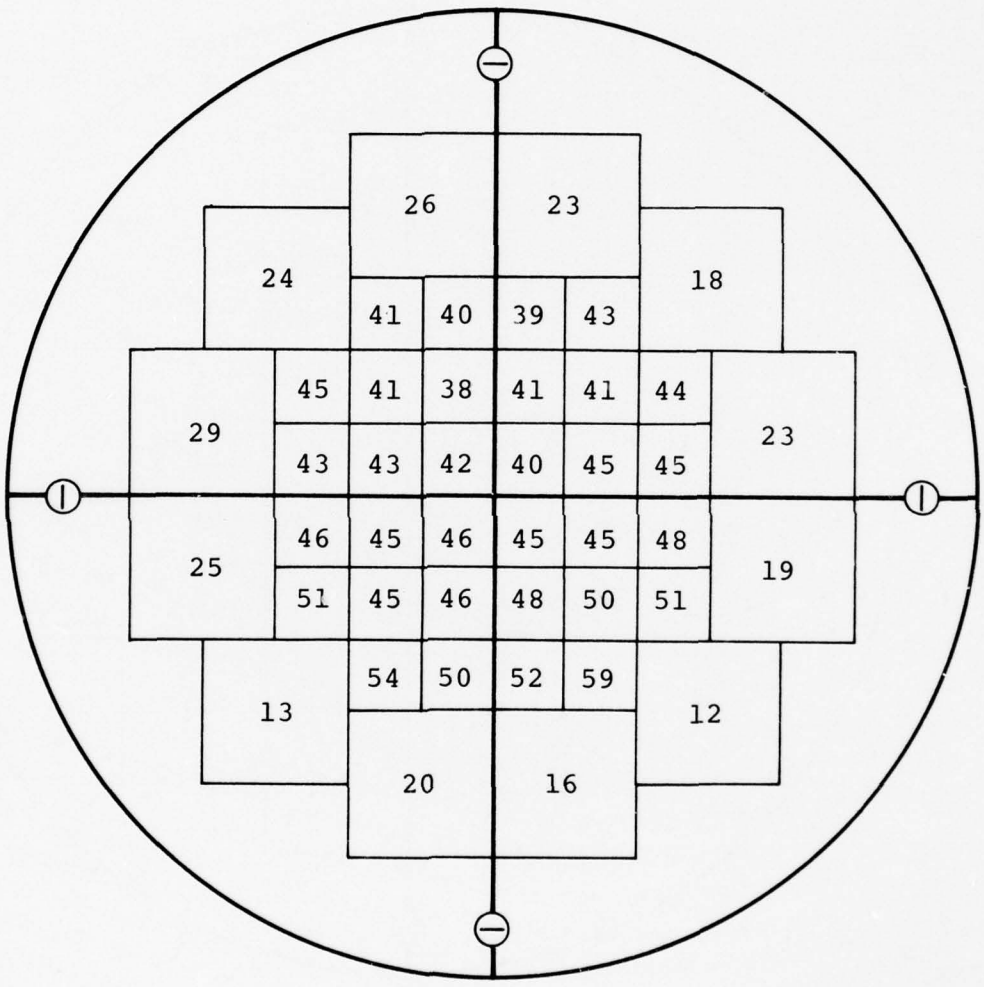

Average fluence
over central 32 square inches = 44 cal/cm^2 ±10% MSD

Energy deposited = 64.3 kJ

Figure B-4 Fluence map, pulse 1980.

Top

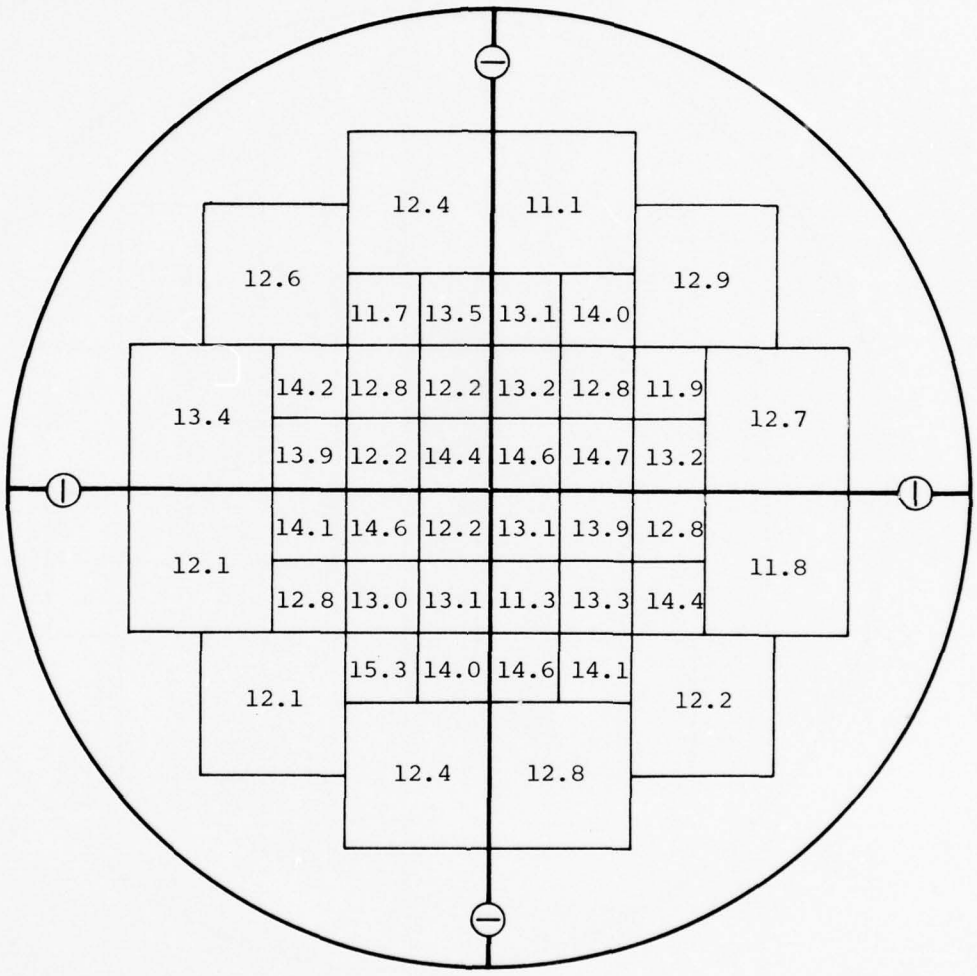

Average fluence
over central 32 square inches = 13.1 cal/cm^2 ± 7% MSD

Energy deposited = 27 kJ

Figure B-5 Fluence map, pulse 1985.

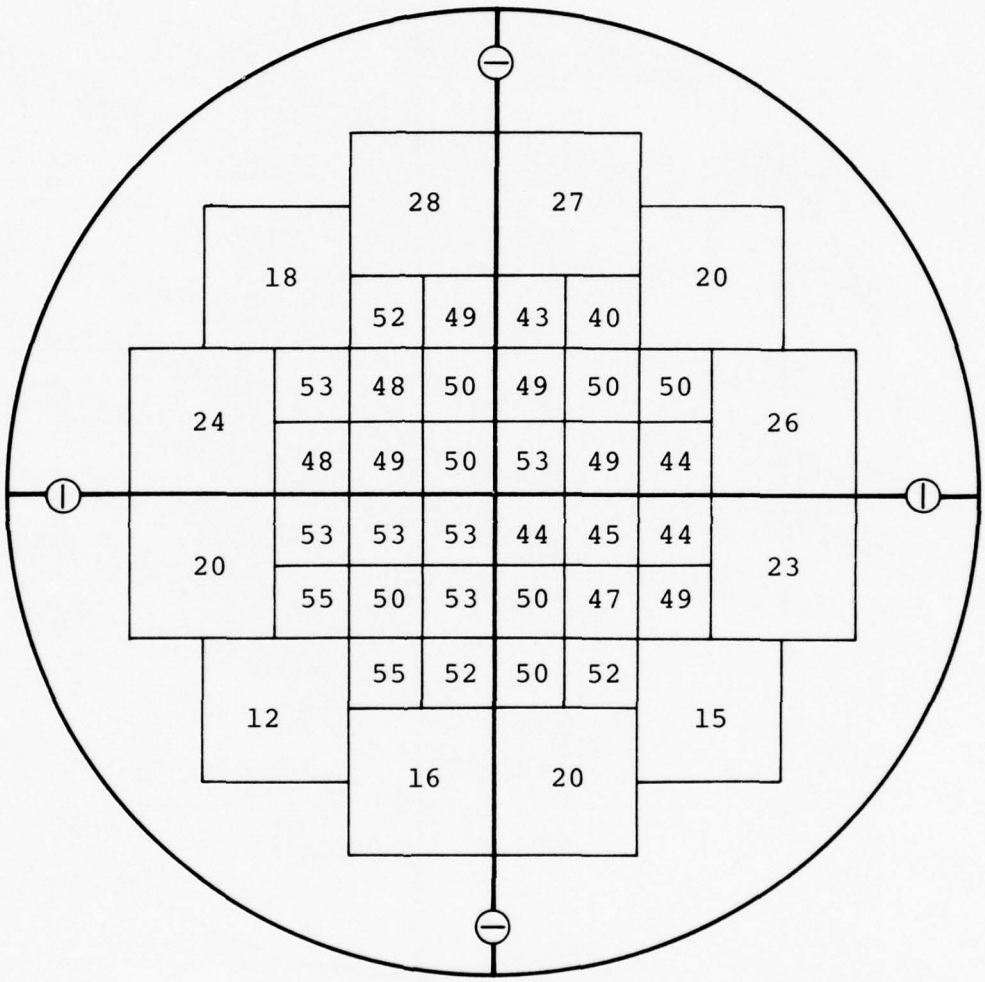

Average fluence
over central 32 square inches = 49 cal/cm^2 ±7% MSD

Energy deposited = 68 kJ

Figure B-6 Fluence map, pulse 2000.

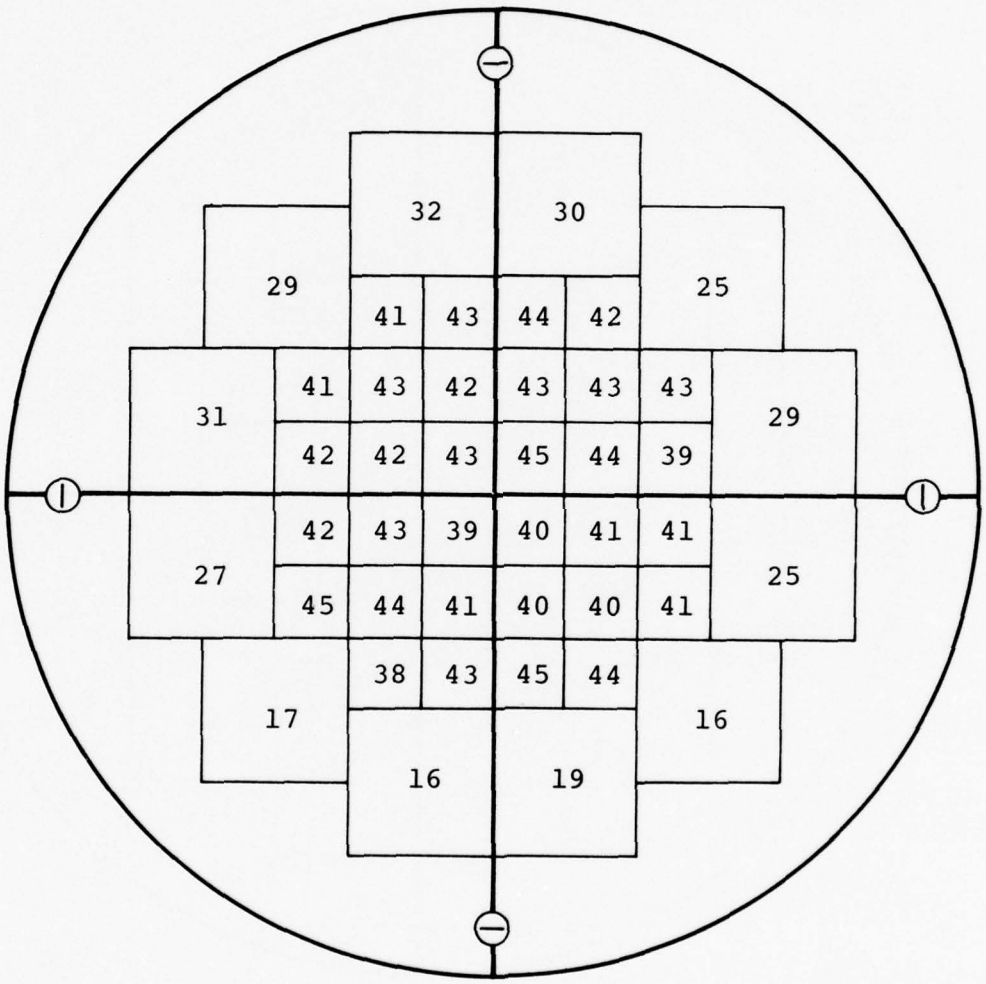

Average fluence
over central 32 square inches = 41 cal/cm^2 ±4% MSD

Energy deposited = 66.5 kJ

Figure B-7 Fluence map, pulse 2003.

Top

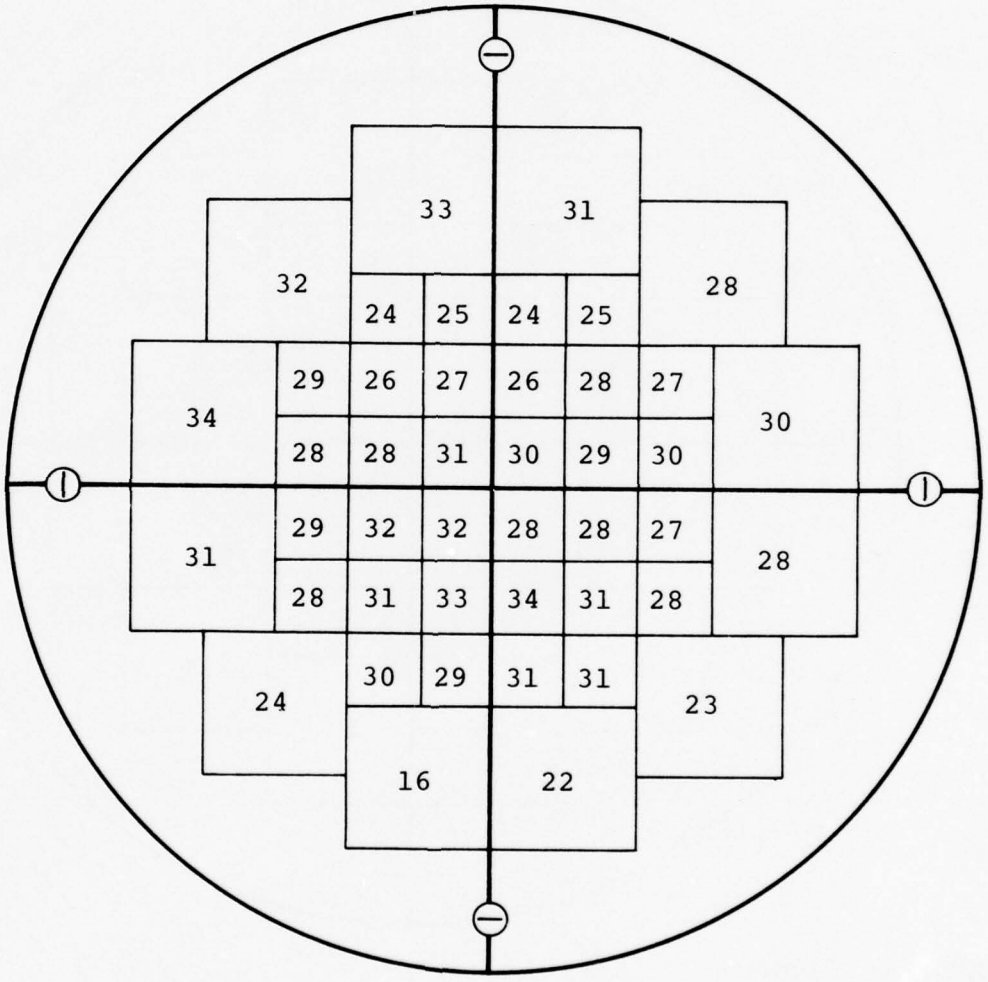

Average fluence
over central 32 square inches = 28 cal/cm^2 ±9% MSD

Energy deposited = 59.3 kJ

Figure B-8 Fluence map, pulse 2004.

Top

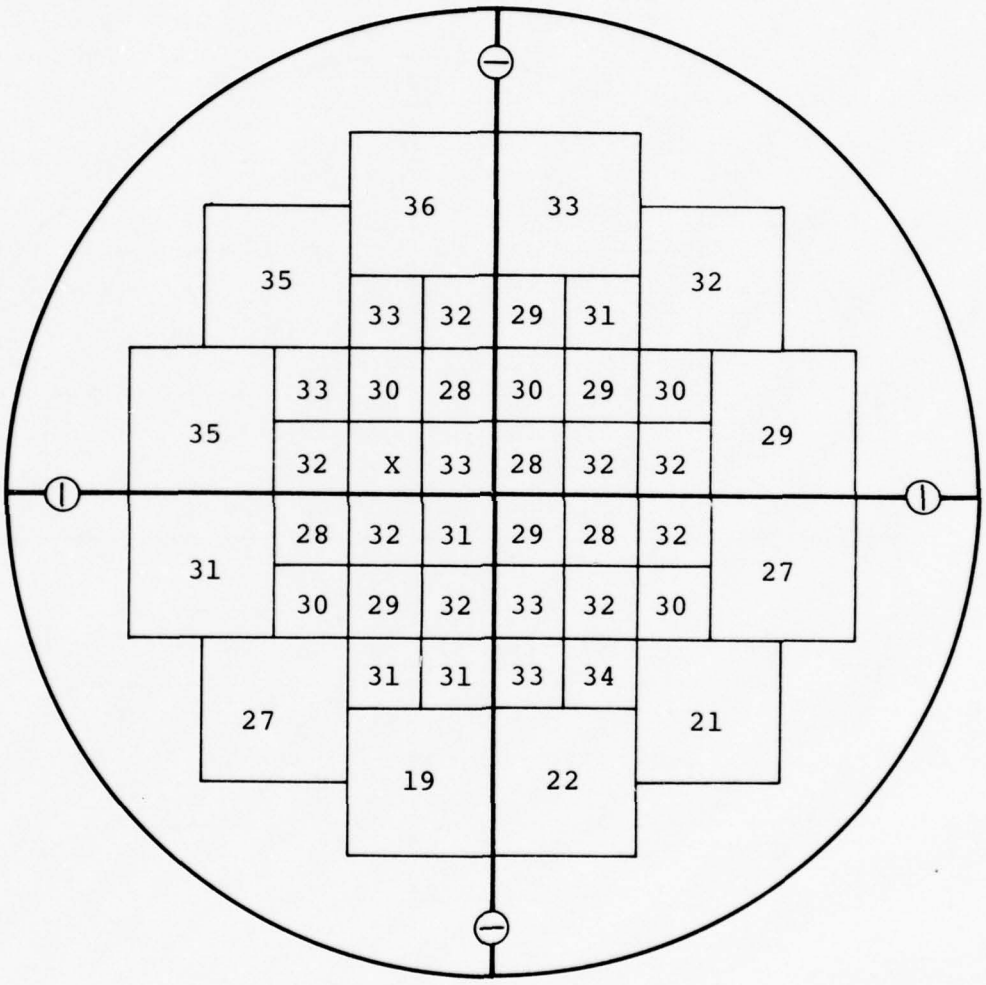

Average fluence
over central 32 square inches = 30 cal/cm^2 ±6% MSD

Energy deposited = 62.5 kJ

Figure B-9 Fluence map, pulse 2006.

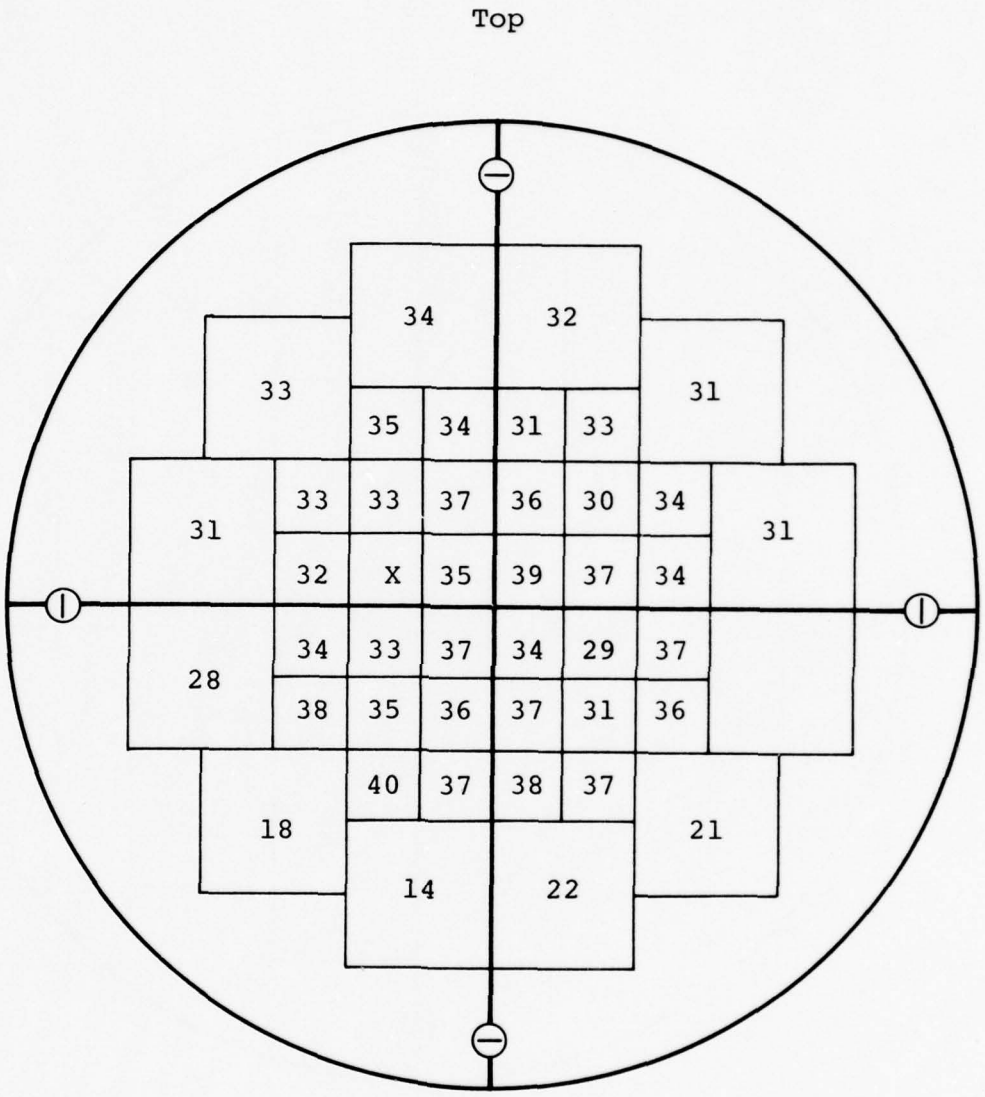

Average fluence
over central 32 square inches = 34 cal/cm^2 ±8% MSD

Energy deposited = 63.6 kJ

Figure B-10 Fluence map, pulse 2007.

Top

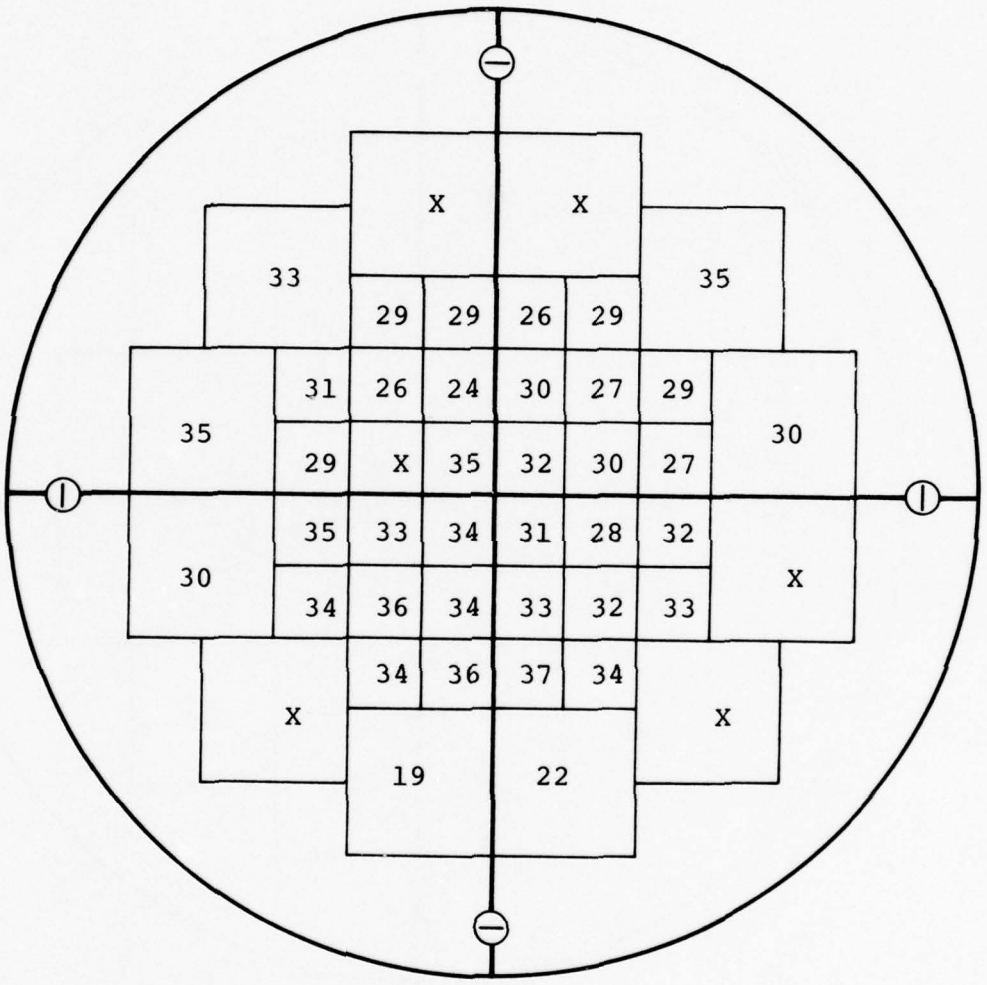

Average fluence
over central 32 square inches = 31 cal/cm^2 ±11% MSD

Energy deposited = ~ 63.2 kJ

Figure B-11 Fluence map, pulse 2009.

Top

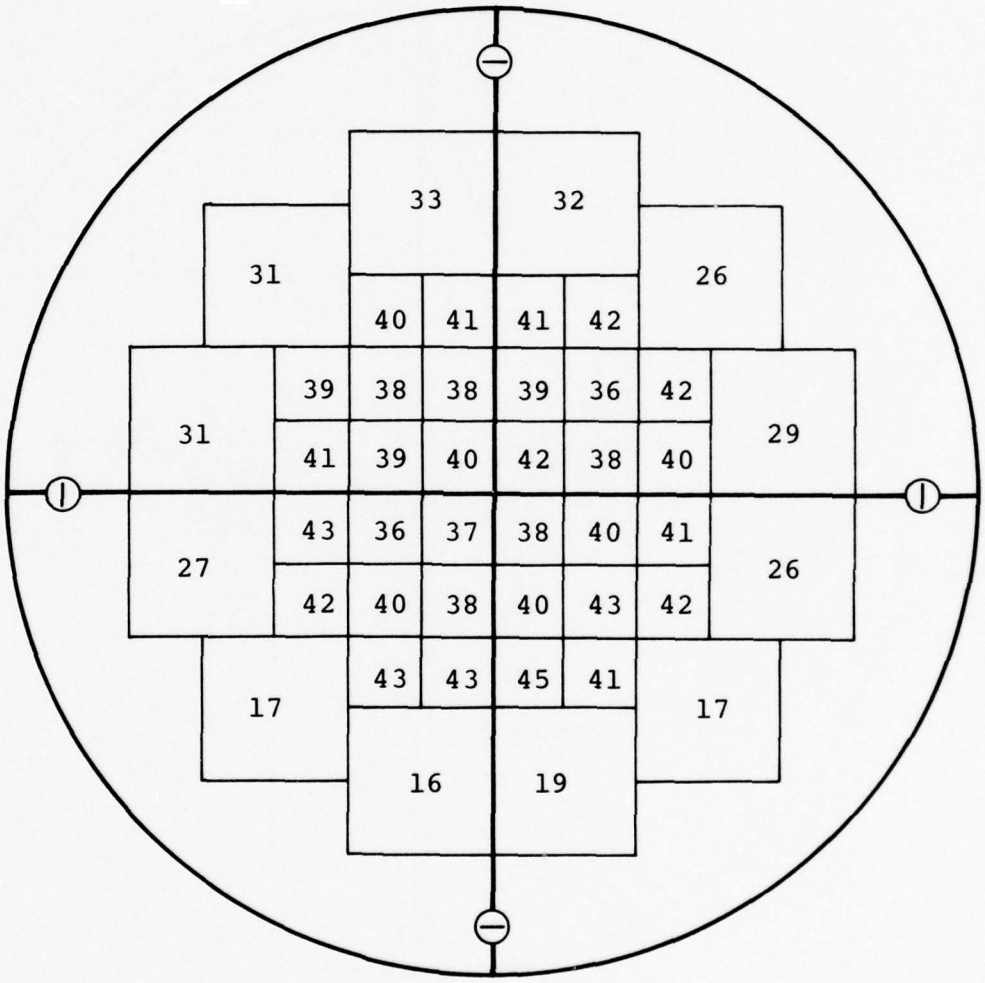

Average fluence
over central 32 square inches = 39 cal/cm^2 ±5% MSD

Energy deposited = 66 kJ

Figure B-12 Fluence map, pulse 2011.

Top

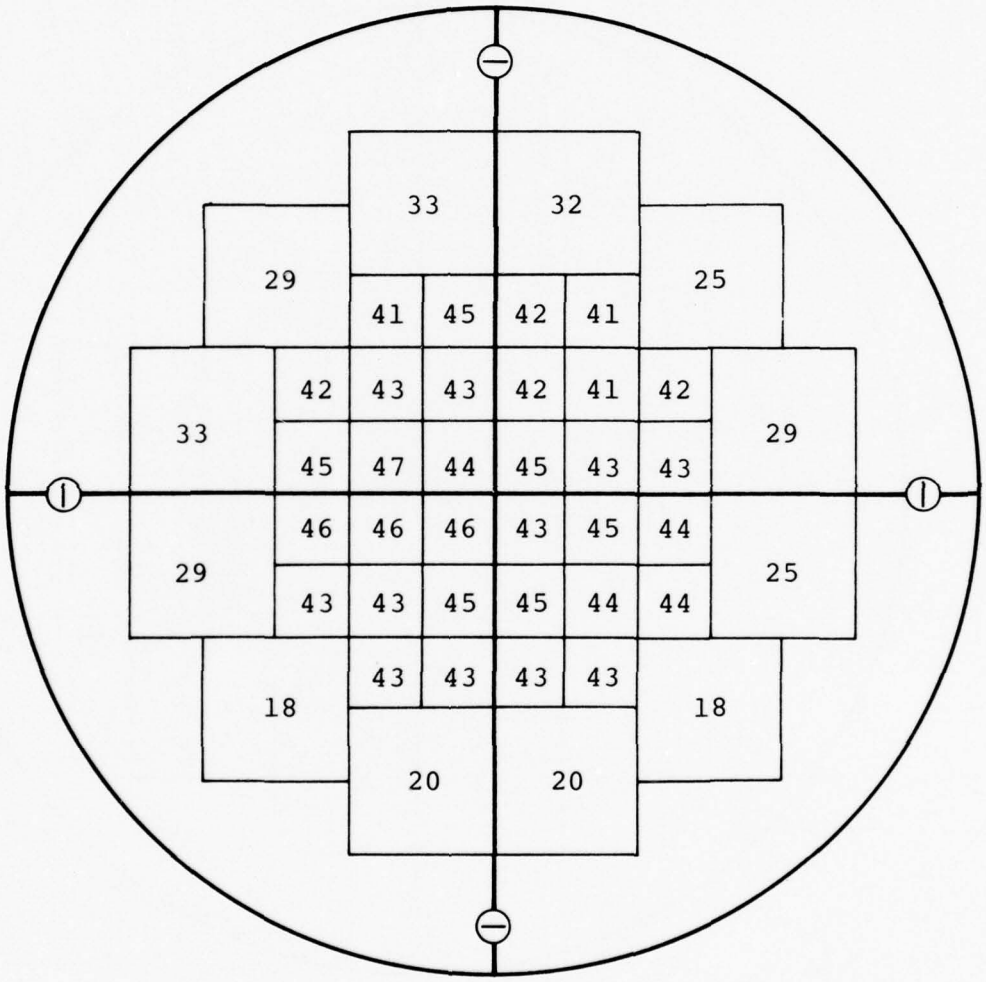

Average fluence
over central 32 square inches = 43 cal/cm^2 ±4% MSD

Energy deposited = 69.3 kJ

Figure B-13 Fluence map, pulse 2013.

Top

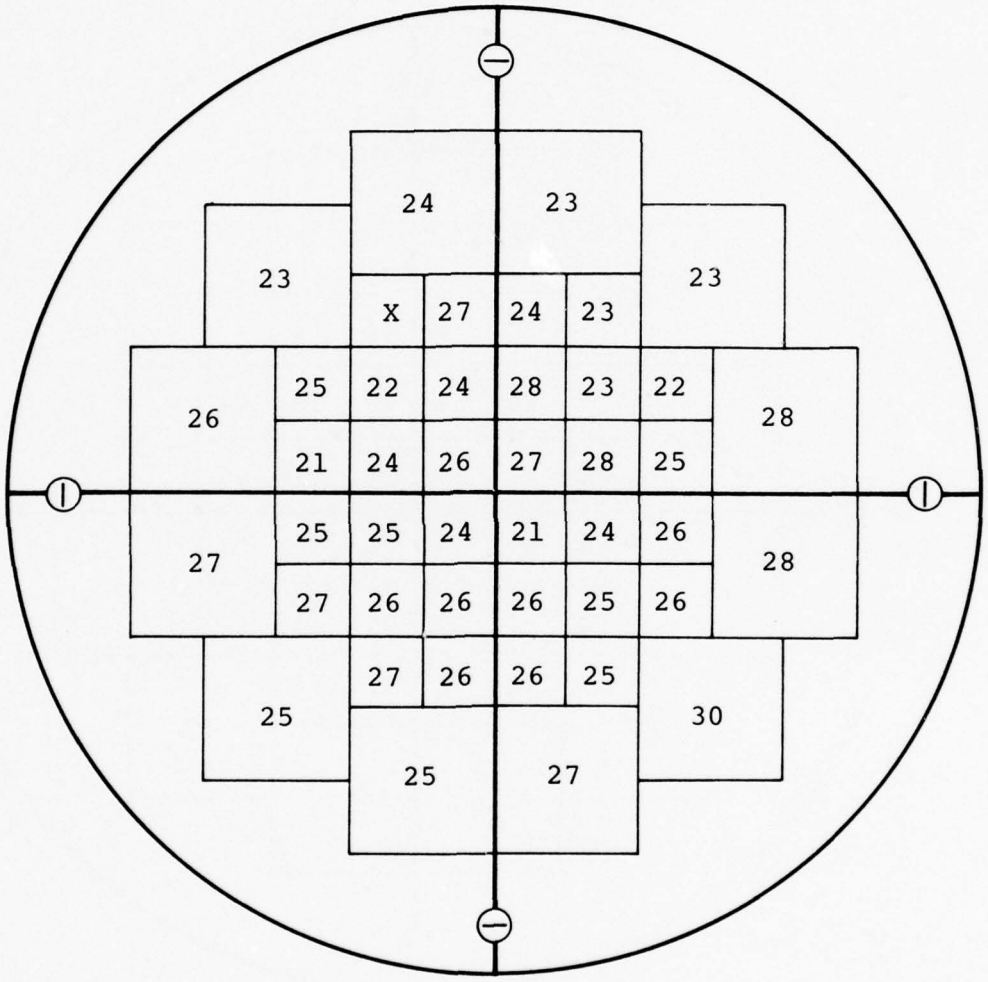

Average fluence
over central 32 square inches = 24 cal/cm^2 ±7% MSD

Energy deposited = 53 kJ

Figure B-14 Fluence map, pulse 2017.

Top

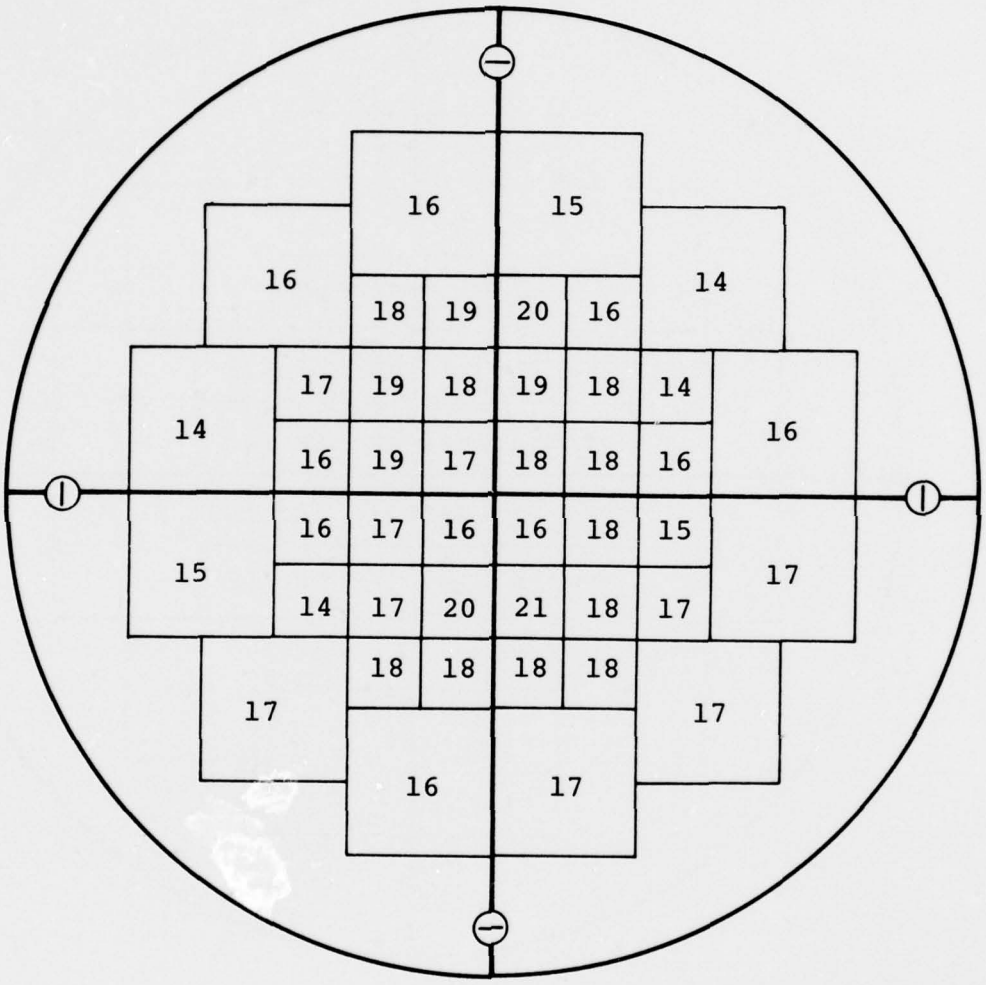

Average fluence
over central 32 square inches = 17 cal/cm^2 ±9% MSD

Energy deposited = 35 kJ

Figure B-15 Fluence map, pulse 2018.

Top

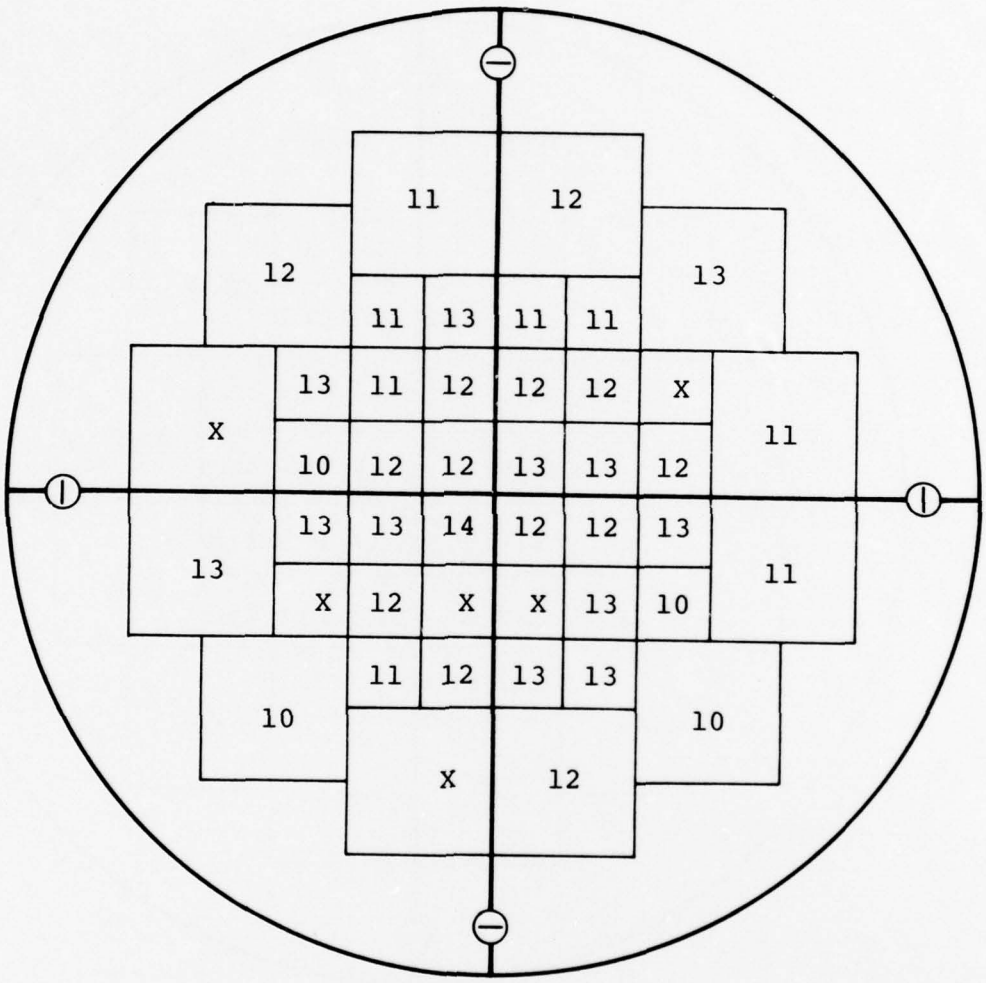

Average fluence
over central 32 square inches=12 cal/cm^2 ±8% MSD
Energy deposited = 21 kJ

Figure B-16 Fluence map, pulse 2019.

Top

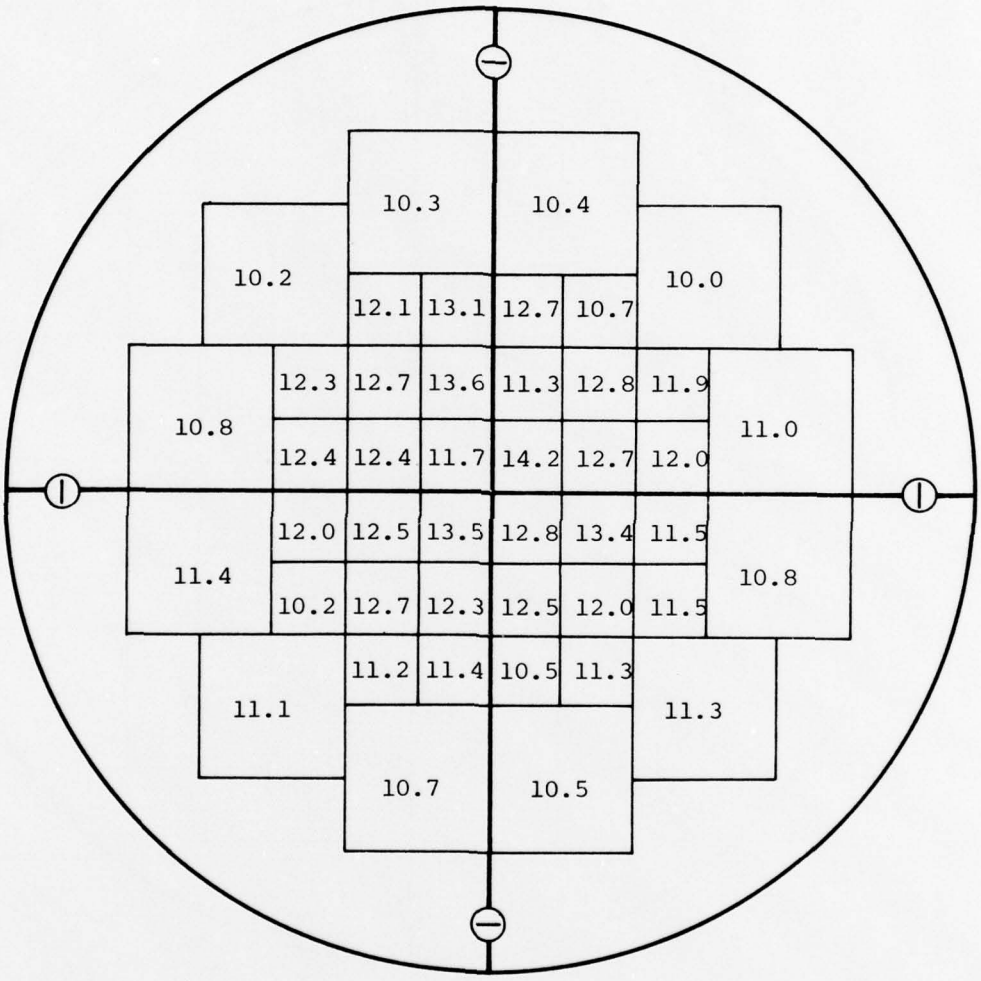

Average fluence
over central 32 square inches = 11.9 cal/cm^2 ±7% MSD

Energy deposited = 24 kJ

Figure B-17 Fluence map, pulse 2020.

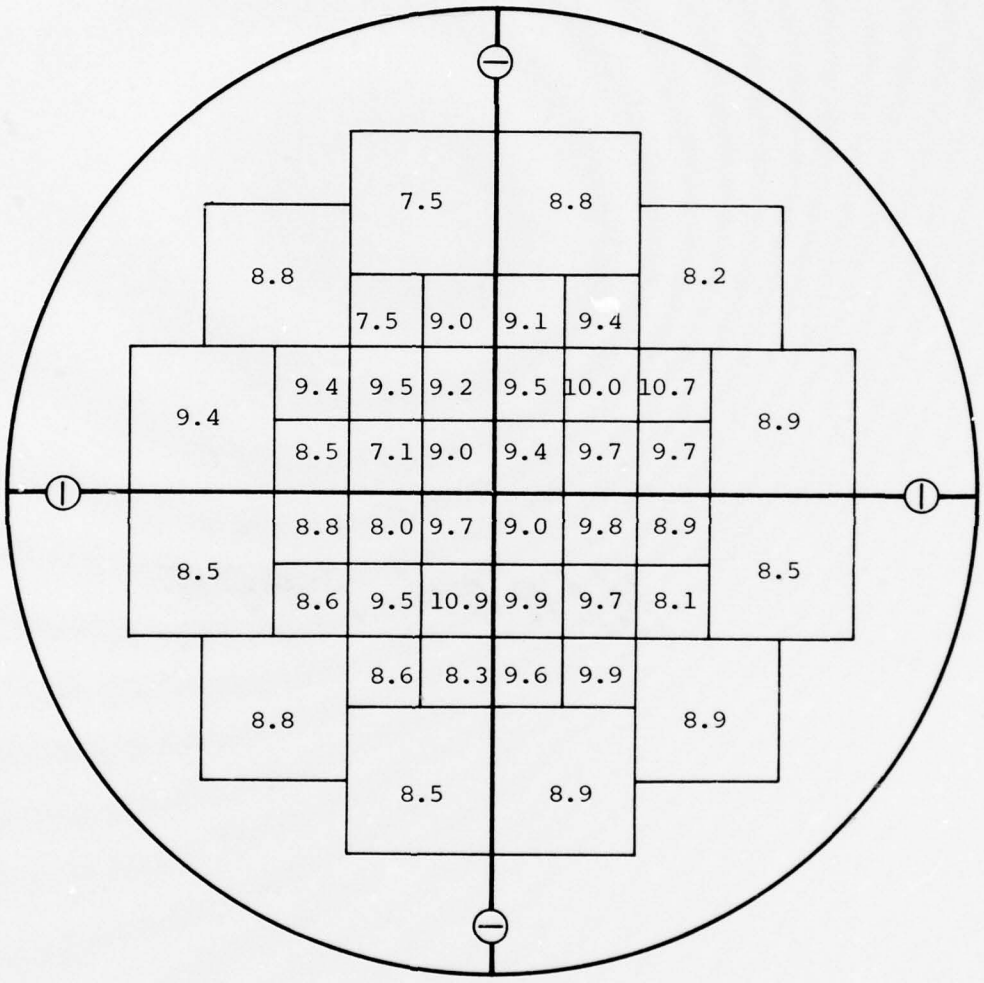

Average fluence
over central 32 square inches = 9 cal/cm^2 ±9% MSD

Energy deposited = 19 kJ

Figure B-18 Fluence map, pulse 2022.

APPENDIX C

MEASURED ELECTRON BEAM ENERGY DEPOSITION PROFILES

This Appendix presents the individual electron beam energy deposition profiles measured in this program.

The data for pulse 2016 has been deleted because the thermocouple on the first foil developed an open circuit. The calorimeter was then rebuilt and on successive pulses (2021 and 2023) the data was peculiar. For these pulses, the correlation with calculations was poor, so the calorimeter was disassembled for inspection. The thermocouples for the first two foils were found to be shorted together inside the calorimeter.

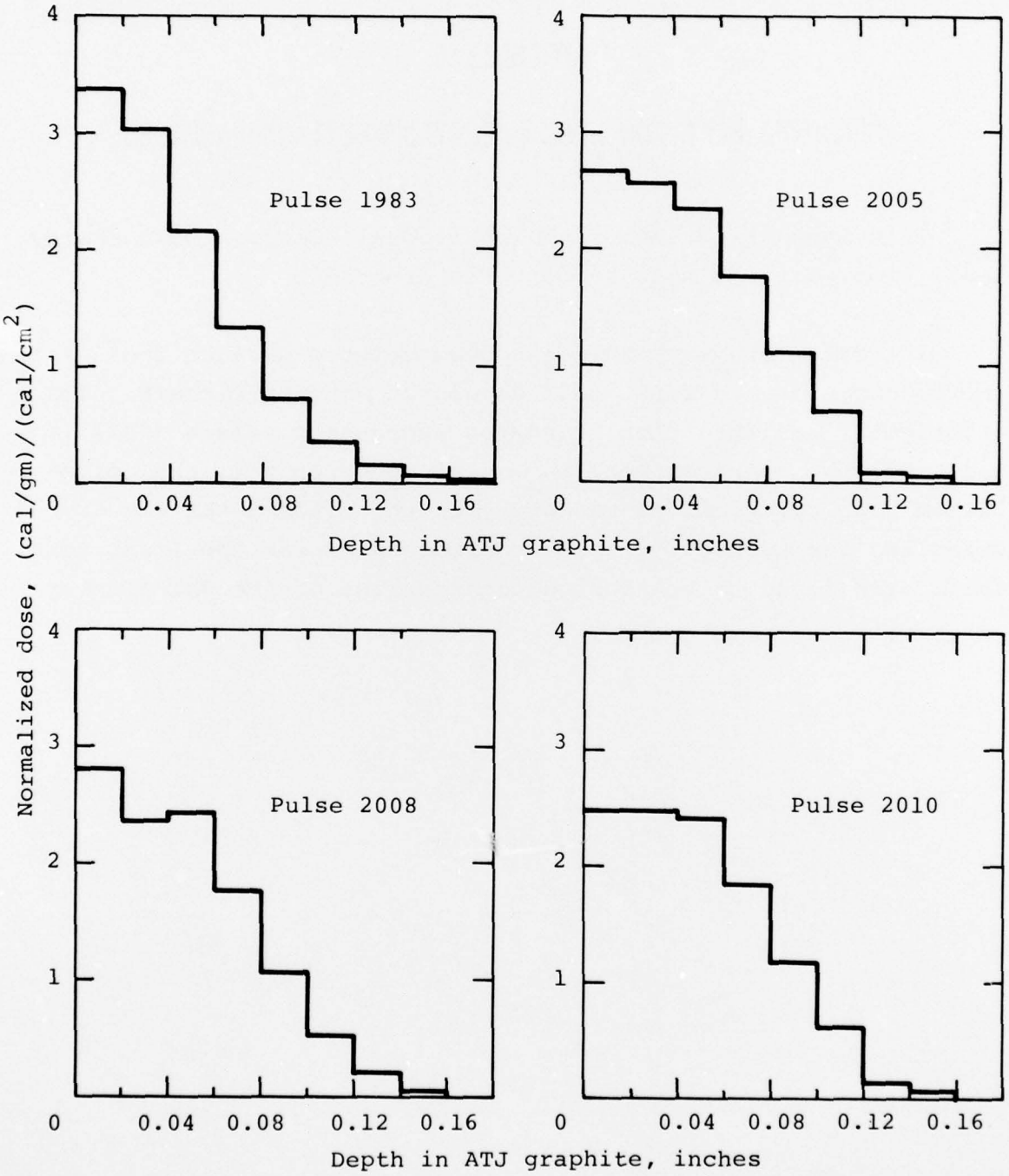

Figure C-1 Measured electron beam energy deposition profiles.

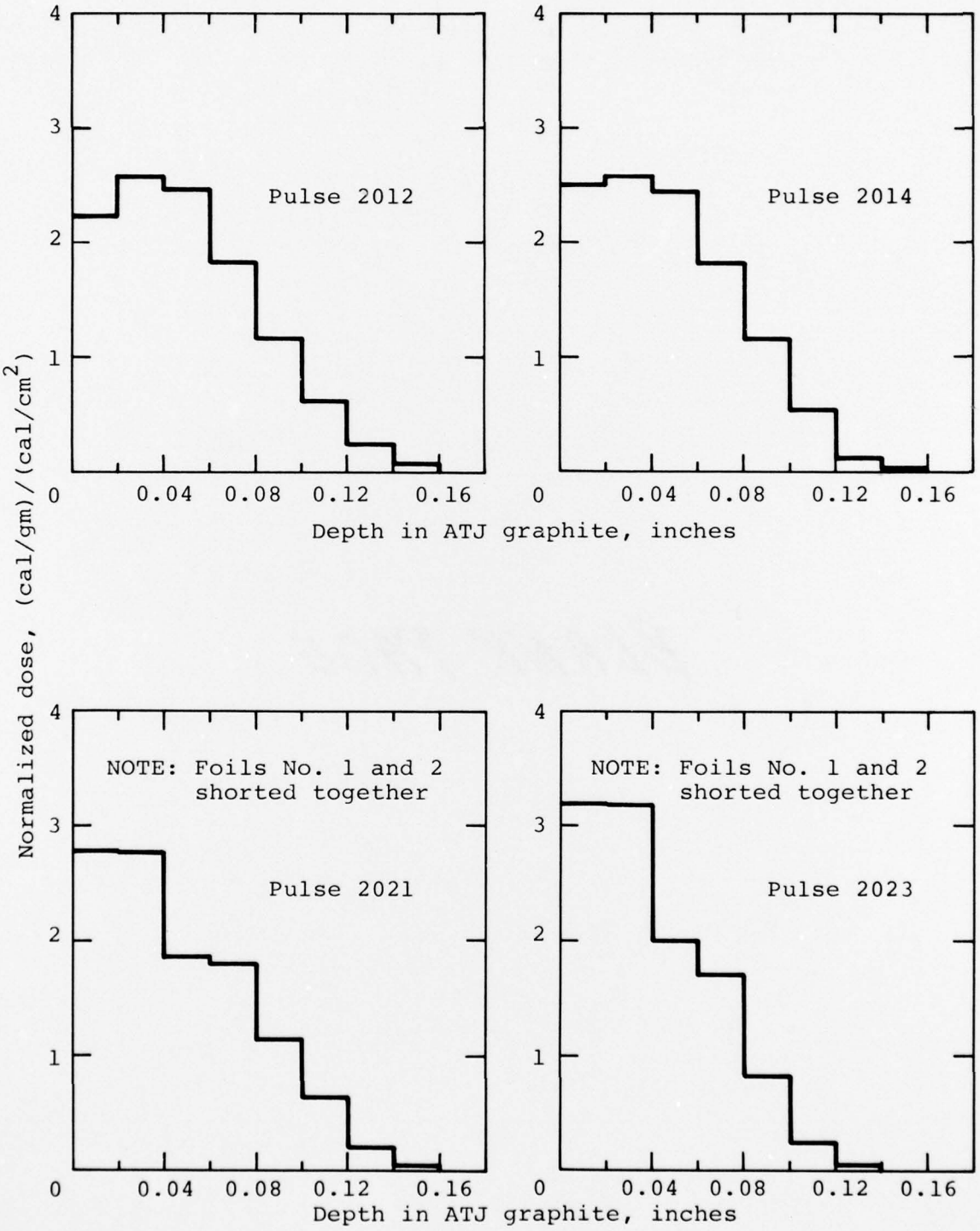

Figure C-2 Measured electron beam energy deposition profiles.

APPENDIX D

ON-LINE DATA ANALYSIS

It is a time-consuming task to produce the detailed analysis required for beam characterization. During a thermal-structural response program, it is necessary to know the electron beam loading conditions "on-line" so that appropriate changes can be made for subsequent pulses. The data listed in Table 1 were used to develop the on-line technique.

The correlation found between calculated fluence and measured fluence was very encouraging (see Figure 7). There were (small) pulse-to-pulse variations in beam energy in the diode, so the data were normalized by the beam energy in the diode (Figure D-1)

$$N\phi_C = \frac{0.81\ NE_D\ L}{A_C}$$

$$N\phi_M = \frac{\phi_M}{E_D}$$

where

$N\phi_C$ is normalized calculated fluence (cal/cm^2)/kJ in diode

0.81 is transport efficiency

NE_D is normalized beam energy in the diode, 240 calories (1 kJ)

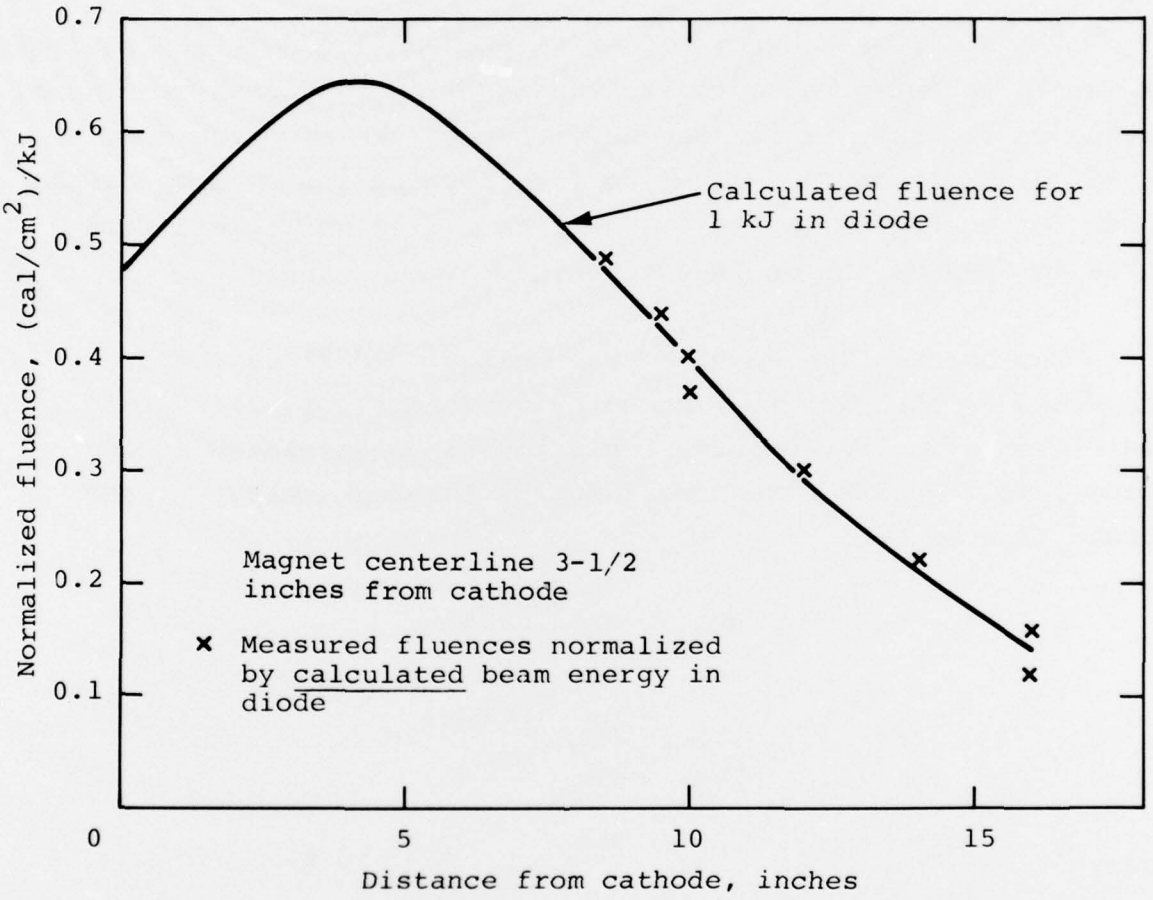

Figure D-1 Normalized fluence, using calculated beam energy in diode.

L is lens ratio

A_c is cathode area (410 cm^2)

$N\phi_M$ is normalized measured fluence (cal/cm^2)/kJ

ϕ_M is measured fluence

E_D is diode energy in kJ

This correlation, though more aesthetically pleasing than that shown in Figure 7, is not appreciably better; the measurements agree with the calculated values to ±7 percent MSD. However, this correlation does allow estimation of fluence for pulses which do have different beam energy in the diode (for example pulse 2019), if the beam energy in the diode is known.

The beam energy in the diode could be estimated to ±7 percent MSD from the peak power determined in the laboratory;

$$E_D\text{est} = 0.13 \underbrace{V_c * I}_{\text{laboratory estimate of peak power}}$$

where

$E_D$est is the estimated energy in the diode in kJ

0.13 is the proportionality constant

V_c is the peak acceleration voltage in MV (oscilloscope data)

I is the diode current in kA at peak acceleration voltage (oscilloscope data)

All of the fluence measurements taken with the magnet centerline 3½ inches from the cathode were normalized, using the energy in the diode (estimated from VC and I) and are compared with the calculated value in Figure D-2. The correlation is good, except for data collected in the center of the lens. Pulse 2013 is treated separately (see Appendix E).

The data in the center of the lens had the same transport efficiency as the other data (approximately 80 percent), but the average fluence is lower than the estimated fluence by approximately 22 percent. This discrepancy suggests that the fluence distribution near the center of the lens is anomalous. The anomalous fluence distribution was not pursued in this program because the fluence levels of interest for the proposed DNA-LMSC thermal-structural response program are found in the diverging portion of the lens, where the beam is well-behaved.

There was not enough data to develop an on-line technique for estimating electron beam energy deposition profiles, but it was found that the mean electron energy was $0.68*VC^{max}$ (±3 percent MSD).

Using these techniques, the fluence and mean electron energy can be estimated in the laboratory so that beam parameters can be adjusted to achieve appropriate loading conditions on subsequent pulses.

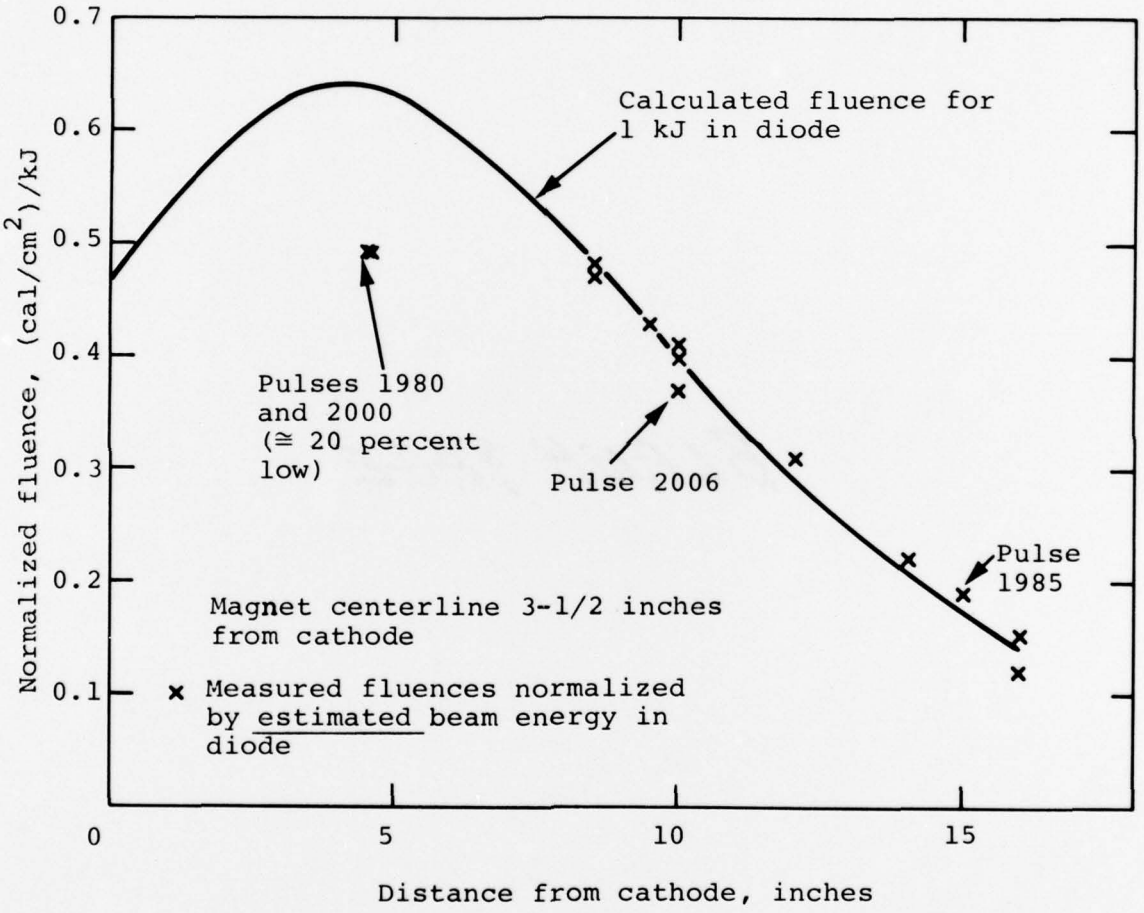

Figure D-2 Normalized fluence, using estimated beam energy in diode.

APPENDIX E

PULSE 2013

On pulse 2013, the accelerator triggered early--approximately 8 msec after the magnet bank was triggered, instead of approximately 15 msec--because of an equipment malfunction. This resulted in a lower magnetic guide field (approximately two-thirds of the usual value) and a change in lens ratio (from approximately 1.03 to approximately 1.20 at 8½ inches from the cathode). The increase in lens ratio is caused by conductors near the cathode, which put the magnetic field near the cathode out of phase with the magnetic field at target location.

Using the appropriate lens ratio and the beam energy in the diode (estimated from VC and I) the calculated fluence is 41 cal/cm^2, which compares favorably with the measured fluence of 43 cal/cm^2.

DISTRIBUTION LIST

DEPARTMENT OF DEFENSE

Defense Documentation Center
Cameron Station
12 cy ATTN: TC

Director
Defense Intelligence Agency
ATTN: DTICI, Robert I. Rubenstein

Director
Defense Nuclear Agency
ATTN: STVL
ATTN: RAEV
ATTN: TISI, Archives
3 cy ATTN: TITL, Tech. Library
ATTN: DDST

Under Secretary of Def. for Rsch. & Engrg.
ATTN: S&SS (OS)

Commander
Field Command
Defense Nuclear Agency
ATTN: FCPR

Director
Joint Strat. Tgt. Planning Staff, JCS
ATTN: JSAS

Chief
Livermore Division, Fld. Command, DNA
Lawrence Livermore Laboratory
ATTN: FCPRL

DEPARTMENT OF THE ARMY

Commander
BMD System Command
ATTN: SSC-TEN

Dep. Chief of Staff for Rsch. Dev. & Acq.
ATTN: DAMA-CSM-N

Commander
Harry Diamond Laboratories
ATTN: DRXDO-RBH, Paul A. Caldwell
ATTN: DELHD-RCC, John A. Rosado
ATTN: DELHD-NP
ATTN: DRXDO-TI, Tech. Library

Commander
Picatinny Arsenal
ATTN: SMUPA ND-N-E

Commander
Redstone Scientific Information Ctr.
U.S. Army Missile Command
3 cy ATTN: Chief, Documents

Commander
U.S. Army Missile Command
ATTN: DRCPM-PE-EA

DEPARTMENT OF THE ARMY (Continued)

Commander
U.S. Army Nuclear Agency
ATTN: ATCN-W

Commander
U.S. Army Test and Evaluation Command
ATTN: DRSTE-EL

DEPARTMENT OF THE NAVY

Chief of Naval Operations
ATTN: Robert A. Blaise, 604C4

Commander
Naval Electronic Systems Command
ATTN: Code 5032

Commanding Officer
Naval Intelligence Support Center
ATTN: NISC-45

Director
Naval Research Laboratory
ATTN: John Davis, Code 5410
ATTN: Gerald Cooperstein, Code 7770
ATTN: Jack D. Brown, Code 7701

Officer-in-Charge
Naval Surface Weapons Center
ATTN: Navy Nuc. Prgms. Off., Code WA501
ATTN: Code WR43

Commander
Naval Weapons Center
ATTN: Code 533, Tech. Library

DEPARTMENT OF THE AIR FORCE

AF Weapons Laboratory, AFSC
ATTN: ELC
ATTN: NT
ATTN: SUL
ATTN: DYP
ATTN: CA

Hq USAF/RD
ATTN: RDQSM

SAMSO/DY
ATTN: DYS

SAMSO/IN
ATTN: IND, Maj Darryl S. Muskin

SAMSO/MN
ATTN: MNNH

SAMSO/SK
ATTN: SKF, Peter H. Stadler

DEPARTMENT OF ENERGY

University of California
Lawrence Livermore Laboratory
ATTN: L-18
ATTN: L-153
ATTN: Tech. Info., Dept. L-3
ATTN: John Nuckolls, A Div. L-545

Sandia Laboratories
ATTN: Doc. Con. for 3141, Sandia Rpt. Coll.
ATTN: Doc. Con. for 5240, Gerald Yonas

DEPARTMENT OF DEFENSE CONTRACTORS

Avco Research & Systems Group
ATTN: Research Lib., A830, Rm. 7201

The BDM Corporation
ATTN: Technical Library

The Boeing Company
ATTN: Aerospace Library

Dikewood Industries, Inc.
ATTN: L. Wayne Davis

EG&G, Inc.
ATTN: Technical Library

Ford Aerospace & Communications Corp.
ATTN: Library
ATTN: Donald R. McMorrow, MS G30

Ford Aerospace & Communications Operations
ATTN: Tech. Info. Section

General Electric Company
Space Division
ATTN: Joseph C. Peden, VFSC, Rm. 4230M

General Electric Company
TEMPO-Center for Advanced Studies
ATTN: DASIAC

Institute for Defense Analyses
ATTN: IDA Librarian, Ruth S. Smith

ION Physics Corporation
ATTN: H. Milde

IRT Corporation
ATTN: R. L. Mertz

Jaycor
ATTN: Eric P. Wenaas

Jaycor
ATTN: Robert Sullivan

Kaman Sciences Corporation
ATTN: Donald H. Bryce
ATTN: Walter E. Ware
ATTN: Albert P. Bridges
ATTN: John R. Hoffman

Lockheed Missiles and Space Co., Inc.
ATTN: Lloyd F. Chase

DEPARTMENT OF DEFENSE CONTRACTORS (Continued)

Maxwell Laboratories, Inc.
ATTN: A. Richard Miller
ATTN: Peter Korn
ATTN: Alan C. Kolb

McDonnell Douglas Corporation
ATTN: Stanley Schneider

Mission Research Corporation
ATTN: Conrad L. Longmire
ATTN: William C. Hart

Mission Research Corporation
ATTN: V. A. J. Van Lint

Northrop Corporation
Northrop Research and Technology Center
ATTN: Library

Northrop Corporation
Electronic Division
ATTN: Vincent R. Demartino

Physics International Company
ATTN: Doc. Con. for Charles H. Stallings
ATTN: Doc. Con. for Bernard H. Bernstein
ATTN: Doc. Con. for Philip W. Spence
ATTN: Doc. Con. for Sidney D. Putnam
ATTN: Doc. Con. for Kendall Childers
ATTN: Doc. Con. for Ian D. Smith

Pulsar Associates, Inc.
ATTN: Carleton H. Jones, Jr.

R & D Associates
ATTN: C. MacDonald
ATTN: William R. Graham, Jr.
ATTN: Leonard Schlessinger

Science Applications, Inc.
ATTN: J. Robert Beyster

Spire Corporation
ATTN: Roger G. Little

SRI International
ATTN: Setsuo Ddairiki

Systems, Science and Software, Inc.
ATTN: David A. Meskan

Systems, Science and Software, Inc.
ATTN: Andrew R. Wilson

Texas Tech University
ATTN: Travis L. Simpson

TRW Defense & Space Sys. Group
ATTN: Tech. Info. Center, S-1930

Vought Corporation
ATTN: Technical Library